

# Heavy Quark Diffusion as a Probe of the Quark-Gluon Plasma

Ralf Rapp and Hendrik van Hees  
Cyclotron Institute and Physics Department, Texas A&M University  
College Station, Texas 77843-3366, U.S.A.

October 25, 2018

## Abstract

In this article we report on recent research on the properties of elementary particle matter governed by the strong nuclear force, at extremes of high temperature and energy density. At about  $10^{12}$  Kelvin, the theory of the strong interaction, Quantum Chromodynamics (QCD), predicts the existence of a new state of matter in which the building blocks of atomic nuclei (protons and neutrons) dissolve into a plasma of quarks and gluons. The Quark-Gluon Plasma (QGP) is believed to have prevailed in the Early Universe during the first few microseconds after the Big Bang. Highly energetic collisions of heavy atomic nuclei provide the unique opportunity to recreate, for a short moment, the QGP in laboratory experiments and study its properties. After a brief introduction to the basic elements of QCD in the vacuum, most notably quark confinement and mass generation, we discuss how these phenomena relate to the occurrence of phase changes in strongly interacting matter at high temperature, as inferred from first-principle numerical simulations of QCD (lattice QCD). This will be followed by a short review of the main experimental findings at the Relativistic Heavy Ion Collider (RHIC) at Brookhaven National Laboratory. The data taken in collisions of gold nuclei thus far provide strong evidence that a QGP has indeed been produced, but with rather remarkable properties indicative for an almost perfect liquid with unprecedentedly small viscosity and high opacity. We then discuss how heavy quarks (charm and bottom) can be utilized to quantitatively probe the transport properties of the strongly-coupled QGP (sQGP). The large heavy-quark mass allows to set up a Brownian motion approach, which can serve to evaluate different approaches for heavy-quark interactions in the sQGP. In particular, we discuss an implementation of lattice QCD computations of the heavy-quark potential in the QGP. This approach generates “pre-hadronic” resonance structures in heavy-quark scattering off light quarks from the medium, leading to large scattering rates and small diffusion coefficients. The resonance correlations are strongest close to the critical temperature ( $T_c$ ), suggesting an intimate connection to the hadronization of the QGP. The implementation of heavy-quark transport into Langevin simulations of an expanding QGP fireball at RHIC enables quantitative comparisons with experimental data. The extracted heavy-quark diffusion coefficients are employed for a schematic estimate of the shear viscosity, corroborating the notion of a strongly-coupled QGP in the vicinity of  $T_c$ .

# 1 Introduction

## 1.1 Elementary Particles and Forces

The quest for the elementary constituents from which the matter around us is built has always fascinated mankind. In the fifth century B.C., Greek philosophers introduced the notion of an *indivisible* entity of matter, the  $\alpha\tau\omicron\mu\omicron\sigma$  (atom). More than 2000 years passed before this concept was systematized in the nineteenth century in terms of the chemical elements as the building blocks of the known substances. The large variety of the chemical elements, however, called for a deeper substructure within these atoms, which were soon revealed as bound states of negatively charged electrons ( $e^-$ ) and positively charged atomic nuclei, held together by their mutual attraction provided by the electromagnetic force. The nuclei, while very small in size (but carrying about 99% of the atom's mass), were found to further decompose in positively charged protons ( $p$ ) and uncharged neutrons ( $n$ ), both of approximately equal mass,  $M_{p,n} \simeq 0.94 \text{ GeV}/c^2$ . This was a great achievement, since at this point all matter was reduced to 3 particles:  $p$ ,  $n$ ,  $e^-$ . There was still the problem of the stability of the atomic nucleus, since packing together many positive charges (protons) in a small region of space obviously implies a large electric repulsion. The solution to this problem triggered the discovery of the Strong Nuclear Force acting between nucleons (protons and neutrons); it turned out to be a factor of  $\sim 100$  stronger than the electromagnetic one, but with a very short range of only a few femtometer ( $1 \text{ fm} = 10^{-15} \text{ m}$ ). In the 1950's and 1960's, rapid progress in particle accelerator technology opened new energy regimes in collision experiments of subatomic particles (e.g.,  $p$ - $p$  collisions). As a result, many more particles interacting via the Strong Force (so-called hadrons) were produced and discovered, including "strange" hadrons characterized by a for strongly interacting particles untypically long lifetime. Again, this proliferation of states (the "hadron zoo") called for yet another simplification in terms of hadronic substructure. Gell-Mann introduced three types of "quarks" [1] as the elementary constituents from which all known hadrons could be built; they were dubbed up ( $u$ ), down ( $d$ ) and strange ( $s$ ) quarks, with fractional electric charges  $+2/3$ ,  $-1/3$  and  $-1/3$ , respectively. In this scheme, hadrons are either built from 3 quarks (forming baryons, e.g.,  $p = (uud)$ ,  $n = (udd)$ ), or a quark and an antiquark (forming mesons, e.g.,  $\pi^+ = (u\bar{d})$  or  $K^0 = (d\bar{s})$ ). Three more heavy quark "flavors", carrying significantly larger masses than the light quarks ( $u$ ,  $d$ ,  $s$ ), were discovered in the 1970's – charm ( $c$ ) and bottom ( $b$ ) – as well as in 1995 – the top ( $t$ ) quark.

The discovery of an increasingly deeper structure of the fundamental matter particles is intimately related to the question of their mutual forces which, after all, determine how the variety of observed composite particles is built up. The understanding of fundamental *interactions* is thus of no less importance than the identification of the matter constituents. The modern theoretical framework to provide a unified description are Quantum Field Theories (QFTs), which combine the principles of Quantum Mechanics with those of Special Relativity. In QFTs, charged matter particles (fermions of half-integer spin) interact via the exchange of field quanta (bosons with integer spin). The QFT of the Electromagnetic Force is Quantum Electro-Dynamics (QED), where the associated field quantum is the photon ( $\gamma$ )

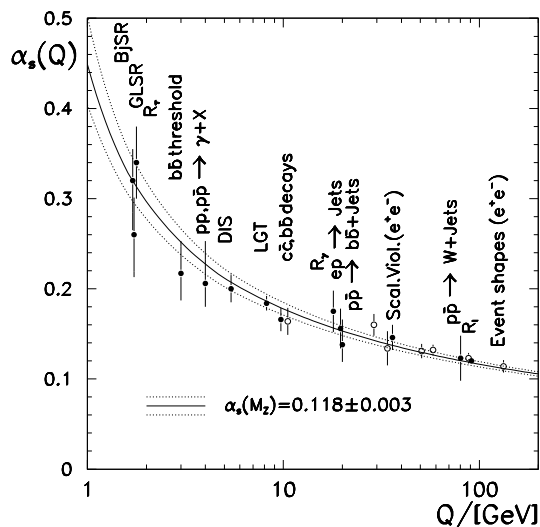


Figure 1: Dependence of the QCD coupling constant,  $\alpha_s = g^2/4\pi$ , on the momentum transfer,  $Q$  (or inverse distance  $1/r \sim Q$ ), of the interaction. Figure taken from Ref. [6].

coupling to electric charges (positive) and anticharges (negative). The coupling constant (or charge) of QED is rather small,  $\alpha_{\text{em}} = e^2/4\pi = 1/137$ , which allows one to organize theoretical calculations in a series of terms characterized by increasing powers of  $\alpha_{\text{em}}$ , so-called perturbation theory. The smallness of  $\alpha_{\text{em}}$  then allows for precise perturbative calculations of electromagnetic observables with an accuracy exceeding ten significant digits for select quantities, rendering QED one of the most successful theories in physics.

The QFT of the strong nuclear force, Quantum Chromo-Dynamics (QCD), has been developed in the early 1970's [2, 3]. The chromo (=color) charge of quarks comes in three variants: red, green and blue (plus their anticharges), rendering QCD a mathematically more involved theory. In particular, the force quanta (“gluons”) themselves carry a nonzero (color-) charge [4], giving rise to gluon self-interactions. The latter are closely related to another remarkable property of QCD, namely the “anti-screening” of its charges in the vacuum: quantum fluctuations, i.e., the virtual quark-gluon cloud around a color charge, induces an increase of the effective charge with increasing distance, a phenomenon known as asymptotic freedom which manifests itself in the running coupling constant (or charge) of QCD,  $\alpha_s(Q)$ , cf. Fig. 1. On the one hand, the interactions at small distances,  $r$  (which, by means of Heisenberg’s uncertainty principle, corresponds to large momentum transfers,  $Q \sim 1/r$ , in a scattering process), are comparatively weak and perturbation theory is applicable (much like in QED). In this regime, QCD is well tested, being in excellent agreement with experiment (albeit not at the same level of precision as QED; even at very large  $Q$ ,  $\alpha_s$  is still a factor of  $\sim 10$  larger than  $\alpha_{\text{em}}$ ). On the other hand, the coupling constant grows toward small  $Q$  entering the realm of “strong QCD” where new *nonperturbative* phenomena occur. Most notably these are the Confinement of color charges and the “Spontaneous

Breaking of Chiral Symmetry” (SBCS). The former refers to the fact that quarks and gluons have never been observed as individual particles, but only come in “colorless” baryons (where the 3 quarks carry an equal amount of the 3 different color charges) or mesons (where quark and antiquark carry color charge and anticharge). Spontaneous Chiral Symmetry Breaking is closely related to the complex structure of the QCD vacuum; the latter is filled with various condensates of quark-antiquark and gluon fields. In particular, the scalar quark condensate of up and down quarks can be quantified by a vacuum expectation value,  $\langle 0|\bar{q}q|0\rangle \simeq (-250 \text{ MeV})^3$ , translating into a total pair density of about 4 per  $\text{fm}^3$ .<sup>1</sup> Thus, the QCD vacuum is a rather dense state, and the quarks inside the hadrons propagating through it acquire an effective mass,  $m_{u,d}^* \simeq 350 \text{ MeV}$ , which is much larger than their bare mass,  $m_{u,d}^0 \simeq 5\text{-}10 \text{ MeV}$ . The QCD condensates are thus the main source of the visible (baryonic) mass in the Universe. The theoretical understanding of the mechanisms underlying Confinement and SBCS, and their possible interrelation, constitutes a major challenge in contemporary particle and nuclear physics research. Currently, the only way to obtain first-principle information on this nonperturbative realm of QCD is through numerical lattice-discretized computer simulations (lattice QCD). However, even with modern day computing power, the numerical results of lattice QCD computations for observable quantities are often hampered by statistical and systematic errors (e.g., due to finite volume and discretization effects); the use of effective models is thus an indispensable tool for a proper interpretation and understanding of lattice QCD results, and to provide connections to experiment.

## 1.2 Elementary Particle Matter and the Quark-Gluon Plasma

A particularly fascinating aspect of the Strong Force is the question of what kind of matter (or phases of matter) it gives rise to. The conventional phases of matter (such as solid, liquid and gas phases of the chemical elements and their compounds, or even electron-ion plasmas) are, in principle, entirely governed by the electromagnetic force. Matter governed by the Strong Force is “readily” available only in form of atomic nuclei: the understanding of these (liquid-like) droplets of nuclear matter (characterized by a mass density of  $\sim 1.67 \cdot 10^{15} \text{ g/cm}^3$ ) is a classical research objective of nuclear physics. But what happens to nuclear matter under extreme compression and/or heating? What happens to the (composite) nucleons? Is it possible to produce truly elementary-particle matter where nucleons have dissolved into their quark (and gluon) constituents (as may be expected from the asymptotic freedom, i.e., small coupling constant, of the quark and gluon interactions at short distance)? Does the condensate structure of the QCD vacuum melt, similar to the condensate of Cooper pairs in a superconductor at sufficiently high temperature? Are there phase transitions associated with these phenomena? The investigation of these questions not only advances our knowledge of strong QCD (including the fundamental problems of

---

<sup>1</sup>In nuclear and particle physics it is common practice to use units of  $\hbar$  (Planck’s constant),  $c$  (speed of light) and  $k$  (Boltzmann constant); in these units, energies, e.g., can be converted into inverse distance by division with  $\hbar c \simeq 197.33 \text{ MeV fm}$ ; energies are also equivalent to temperature.

confinement and mass generation), but also directly relates to the evolution of the early universe, as well as to the properties of extremely compact stellar objects (so-called neutron stars). Lattice-QCD computations at finite temperature indeed predict that hadronic matter undergoes a transition to a state of matter where quarks and gluons are no longer confined into hadrons. The temperature required to induce this transition into the “Quark-Gluon Plasma” (QGP) is approximately  $kT \sim 0.2 \text{ GeV} = 2 \cdot 10^8 \text{ eV}$ , or  $T \sim 10^{12} \text{ K}$ . The Universe is believed to have passed through this transition at about  $10 \mu\text{s}$  ( $=0.00001\text{s}$ ) after its birth. This was, however,  $\sim 15$  billion years ago, and the question arises how one can possibly study the QGP, or more generally the phase diagram of QCD matter, today [5]. Clearly, without input from experiment, this would be a hopeless enterprise.

It turns out that by colliding heavy atomic nuclei at high energies, one can create highly excited strongly interacting matter in the laboratory. The incoming kinetic energy of the colliding nuclei is largely converted into compression and thermal energy, and by varying the collision energy one is able to produce a wide range of different matter types as characterized by their baryon density,  $\rho_B$  and temperature,  $T$ . This is illustrated in a schematic phase diagram of strongly interacting matter in Fig. 2. In the present article we will mainly focus on heavy-ion collisions at the highest currently available energies. These experiments are being conducted at the Relativistic Heavy-Ion Collider (RHIC) at Brookhaven National Laboratory (BNL, Upton, New York): gold (Au) nuclei, fully stripped of their electrons, are accelerated in two separate beam pipes to an energy of  $E = 100 \text{ GeV}$  per nucleon, before being smashed together head on at four collision points where two large (PHENIX and STAR) and two smaller (BRAHMS and PHOBOS) detector systems have been positioned. With each gold nucleus consisting of  $A=197$  nucleons (as given by the atomic mass number of gold), a total (center-of-mass) energy of  $E_{\text{cm}} \simeq 200 A \text{ GeV} \simeq 40 \text{ TeV} = 4 \cdot 10^{13} \text{ eV}$  is brought into the collision zone. Note that the energy of the accelerated nuclei exceeds their rest mass by more than a factor of 100 (recall that the rest mass of the nucleon is  $M_N \simeq 0.94 \text{ GeV}/c^2$ ). In a central Au-Au collision at RHIC approximately 5000 particles are produced (as observed in the detectors), emanating from the collision point with velocities not far from the speed of light. Most of these particles are pions, but essentially all known (and sufficiently long-lived) hadrons made of  $u$ ,  $d$  and  $s$  quarks are observed. The key challenge is then to infer from the debris of produced particles the formation and properties of the matter - the “fireball” - that was created in the immediate aftermath of the collision. While the typical lifetime of the fireball is only about  $\sim 10^{-22}\text{s}$ , it is most likely long enough to form locally equilibrated strongly interacting matter which allows for a meaningful analysis of its properties in terms of thermodynamic concepts, and thus to study the QCD phase diagram as sketched in Fig. 2. This has been largely deduced from the multiplicities and momentum spectra of produced hadrons, which allow to determine typical temperatures and collective expansion velocities of the exploding fireball, at least in the later (hadronic) phases of its evolution. A possibly formed QGP will, however, occur in the earlier (hotter and denser) phases of a heavy-ion reaction. The identification and assessment of suitable QGP signatures is at the very forefront of contemporary research. Hadrons containing heavy quarks (charm and bottom,  $Q = c, b$ ) have been identified as particularly

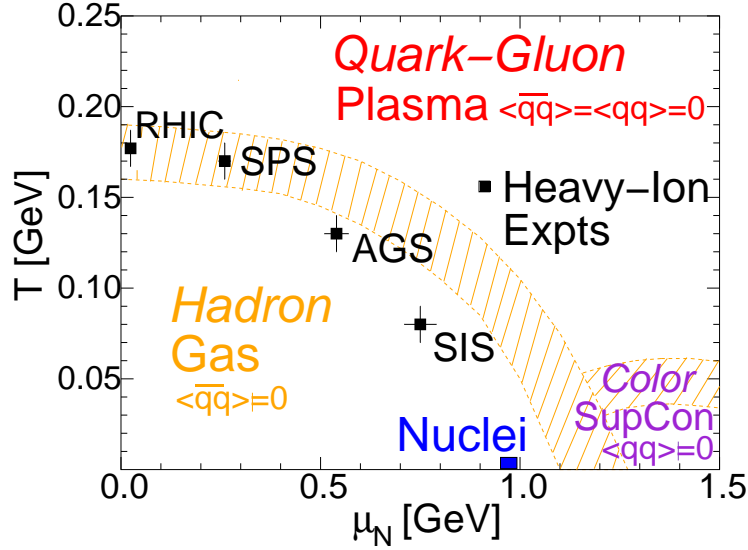


Figure 2: Schematic view of the phase diagram of strongly interacting matter, in terms of the nucleon (or baryon) chemical potential,  $\mu_N$ , and temperature,  $T$ . The former determines the net baryon density in the system. The shaded bands are schematic dividers of the different phases as expected from theoretical model calculations. At vanishing  $\mu_N$ , current lattice QCD calculations indicate a crossover transition from hot hadronic matter to the QGP at a (pseudo-) critical temperature of  $T_c=160-190$  MeV [7, 8]. Normal nuclear matter (as present in atomic nuclei) is located on the  $T=0$  axis at  $\mu_N \simeq 970$  MeV (corresponding to a nucleon density of  $\rho_N \simeq 0.16$  fm $^{-3}$ , the nuclear saturation density). At larger  $\mu_N$  (and small  $T \leq 50-100$  MeV), one expects the formation of a Color-Superconductor [9, 10], i.e., cold quark matter with a BCS-type condensate of quark Cooper pairs,  $\langle 0|qq|0 \rangle \neq 0$ . The “data” points are empirical extractions of  $(\mu_N, T)$ -values from the observed production ratios of various hadron species ( $\pi$ ,  $p$ ,  $K$ ,  $\Lambda$ , etc.) in heavy-ion experiments at different beam energies [11].

promising probes of the QGP. The basic idea is as follows: since charm- and bottom-quark masses,  $m_c \simeq 1.5$  GeV/ $c^2$  and  $m_b \simeq 4.5$  GeV/ $c^2$ , are much larger than the typical temperatures,  $T \simeq T_c \simeq 0.2$  GeV, of the medium formed in a heavy-ion collision, they are (i) only produced very early in the collision (upon first impact of the colliding nuclei) and, (ii) not expected to thermalize during the lifetime of the fireball. Furthermore, the largest changes of their momentum spectra occur when the collision rate and momentum transfer are the highest. This is facilitated by a large density and temperature (i.e., in the early phases of a heavy-ion reaction), but is crucially dependent also on the interaction strength. Both aspects are embodied into the notion of transport coefficients. The main objective of this article is to provide a theoretical description of heavy-quark transport in the QGP, and to test the results in applications to RHIC data.

The remainder of this article is organized as follows: In Sec. 2 we present a general overview of the physics of the Strong Force and the facets of its different matter phases. We start in Sec. 2.1 by introducing basic features of Quantum Chromodynamics (QCD), the quantum field theory describing the strong interactions between quarks and gluons, the elementary building blocks of hadrons. In Sec. 2.2 we briefly review our current understanding of strongly interacting matter and its phase diagram as theoretically expected from both numerical lattice QCD computations and model analysis. In Sec. 2.3 we elucidate the main ideas and achievements of the experimental high-energy heavy-ion programs as conducted at the Relativistic Heavy Ion Collider (RHIC) at the Brookhaven National Laboratory (New York), as well as at the Super Proton Synchrotron (SPS) and the future Large Hadron Collider (LHC) at the European Organization for Nuclear Research (CERN, Geneva, Switzerland). We summarize what has been learned about hot and dense strongly interacting matter thus far, and which questions have emerged and/or remained open. This leads us to the central part of this article, Sec. 3, where we discuss in some detail the theoretical developments and phenomenological applications in using heavy quarks (charm and bottom) as a probe of the Quark-Gluon Plasma. In Sec. 3.1 we concentrate on the theoretical understanding of heavy-quark (HQ) interactions in the QGP. We mostly address elastic scattering, within both perturbative and nonperturbative approaches, where the latter are divided into a resonance model and  $T$ -matrix calculations utilizing potentials extracted from lattice QCD. The HQ interactions in the medium are used to compute pertinent self-energies and transport coefficients for drag and diffusion. In Sec. 3.2 the latter are implemented into a Brownian motion framework of a Fokker-Planck equation which is particularly suitable for describing the diffusion of a heavy particle in a heat bath. In Sec. 3.3 these concepts are applied to heavy-ion collisions, by implementing a Langevin simulation of HQ transport into realistic QGP fireball expansions for Au-Au collisions at RHIC. To make contact with experiment, the quarks have to be hadronized which involves a quark coalescence approach at the phase transition, in close connection to successful phenomenology in light hadron spectra. This is followed by an analysis of transverse momentum spectra of heavy mesons and their electron decay spectra for which experimental data are available. In Sec. 3.4 we recapitulate on the ramifications of the theoretical approach in a broader context of Quark-Gluon Plasma research and heavy-ion phenomenology, and outline future lines of investigation. Sec. 4 contains a brief overall summary and conclusions.

## 2 The Quark-Gluon Plasma and Heavy-Ion Collisions

### 2.1 The Strong Force and Quantum Chromodynamics

The basic quantity which, in principle, completely determines the theory of the strong interaction, is the Lagrangian of QCD,

$$\mathcal{L}_{\text{QCD}} = \bar{q} (i \not{D} - \hat{m}_q) q - \frac{1}{4} G_{\mu\nu} G^{\mu\nu} , \quad (1)$$

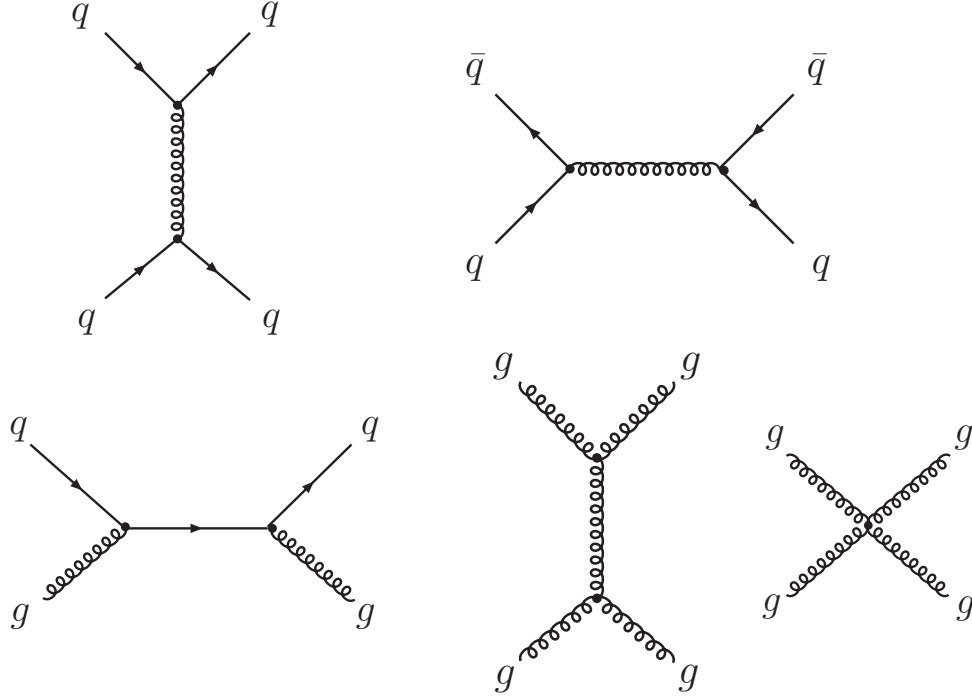


Figure 3: Feynman diagrams for quark-quark scattering via the exchange of a gluon (top left) quark-antiquark scattering via annihilation into a gluon (top right), quark-gluon scattering and gluon-gluon scattering (bottom panels).

where  $q$  and  $\bar{q}$  denote the elementary matter fields, quarks and antiquarks. The quark fields are specified by several quantum numbers: (i) color charge (red, green or blue), (ii) flavor (up, down, strange, charm, bottom and top) and (iii) spin ( $\pm\frac{1}{2}\hbar$ ). The mass matrix  $\hat{m}_q = \text{diag}(m_u, m_d, m_s, m_c, m_b, m_t)$  is a simple diagonal matrix in flavor space. It roughly separates QCD into a light-flavor ( $u, d$  with bare masses  $m_{u,d} \simeq 0.005 \text{ GeV}/c^2$ ) and a heavy-flavor sector ( $c, b, t$  with  $m_c \simeq 1.3 \text{ GeV}/c^2$ ,  $m_b \simeq 4.5 \text{ GeV}/c^2$ ,  $m_t \simeq 175 \text{ GeV}/c^2$ ), while the strange-quark mass is somewhat in between ( $m_s \simeq 0.12 \text{ GeV}/c^2$ ). The interactions of the quarks are encoded in the covariant derivative,  $\mathcal{D} = \partial - ig\mathcal{A}$ , where  $A$  denotes the gluon field, the carrier of the Strong Force, and the gauge coupling  $g$  quantifies the interaction strength as referred to in Fig. 1. A pictorial representation of these interactions can be given in terms of Feynman diagrams: quarks interact via the exchange of gluons, cf. Fig. 3. The gluons are massless particles with spin 1; most notably, they also carry color charge (which comes in 8 different charge-anticharge combinations, e.g., red-antigreen, red-antiblue, etc.), giving rise to gluon self-interactions. These are encoded in the last term of Eq. (1) where  $G_{\mu\nu} = \partial_\mu A_\nu - \partial_\nu A_\mu + g[A_\mu, A_\nu]$ ; the commutator term,  $[A_\mu, A_\nu] = A_\mu \cdot A_\nu - A_\nu \cdot A_\mu$  is a consequence of the  $3 \times 3$  matrix structure in color-charge space and generates 3- and 4-gluon interaction vertices (as depicted in the bottom right panel of Fig. 3). Each interaction



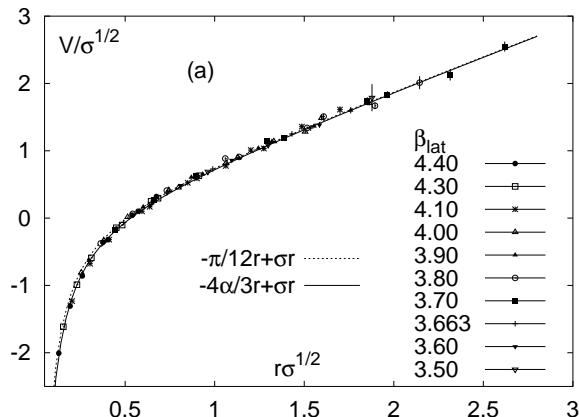


Figure 4: The static potential between a heavy quark and antiquark in vacuum, as a function of their distance, as computed in lattice QCD [13]. Potential and distance are given in units of the string tension,  $\sqrt{\sigma} \simeq 0.42 \text{ GeV} \simeq 2.12 \text{ fm}^{-1}$  (where the conversion has been done using  $\hbar c \simeq 0.197 \text{ GeV fm}$ ).

vertex brings in a factor of  $g$  into the calculations of a given diagram (except for the 4-gluon vertex which is proportional to  $g^2$ ). All diagrams (more precisely, the pertinent scattering amplitudes) shown in Fig. 3 are thus proportional to  $\alpha_s = g^2/4\pi$ , while more complicated diagrams (involving additional quark/gluon vertices) are of higher order in  $\alpha_s$ . This forms the basis for perturbation theory: for small  $\alpha_s$ , higher order diagrams are suppressed, ensuring a rapid convergence of the perturbation series. Perturbative QCD (pQCD) indeed works very well for reactions at large momentum transfer,  $Q$ , where  $\alpha_s(Q)$  is small, cf. Fig. 1, while it breaks down for small  $Q$ . One possibility to obtain information on the nonperturbative interactions is to investigate the potential between two static quark charges, i.e., the potential between a heavy quark and antiquark. In the color neutral channel, a phenomenological ansatz can be written as a combination of a Coulombic attraction at short distances which merges into a linearly rising potential at large distance (signifying confinement),

$$V_{Q\bar{Q}}(r) = -\frac{4\alpha_s}{3r} + \sigma r, \quad (2)$$

where  $\sigma \simeq 1 \text{ GeV/fm}$  denotes the “string tension”. Such a potential provides a good description of the observed spectra of heavy quarkonium states, i.e., charm-anticharm and bottom-antibottom quark bound states. In recent years, the heavy-quark potential has been computed with good precision in lattice QCD, which fully confirmed the phenomenological ansatz, Eq. (2), (see, e.g., Fig. 4). Subsequently, the potential approach, in combination with expansions organized in powers of the inverse HQ mass,  $m_{c,b}$  (rather than the coupling constant), has been developed into an effective theory of low-energy QCD, cf. Ref. [14] for a review.

Besides the (external) quark masses, QCD has only one (intrinsic) dimensionful scale which is generated by quantum effects (loop corrections). The latter give rise to the running coupling constant,

$$\alpha_s(Q) = \frac{1}{(11N_c - 2N_f) \ln(Q^2/\Lambda_{\text{QCD}}^2)}, \quad (3)$$

where  $N_c=3$  is the number of color charges and  $N_f$  the number of active quark flavors at given  $Q$  (i.e., the number of flavors with  $m_q \leq Q$ ). It is tempting to interpret the value of  $\Lambda_{\text{QCD}} = 0.2 \text{ GeV}$  as the dividing line between perturbative and nonperturbative regimes of QCD. In practice, however, the scale for the onset of nonperturbative effects is significantly larger, typically given by the hadronic mass scale of  $\sim 1 \text{ GeV}$ . To understand the emergence of this scale, it is important to realize that the QCD vacuum structure is rather rich, characterized by quark and gluon condensates. E.g., in the light scalar quark-antiquark channel ( $\bar{u}u$  and  $\bar{d}d$ ) a strongly attractive force leads to the spontaneous formation and condensation of  $\bar{q}q$  pairs (reminiscent to a Bose condensate)<sup>2</sup>. An important consequence of the condensate formation is that the light quarks acquire an effective mass when propagating through the condensed vacuum, which is given by the condensate as  $m_q^* \simeq G\langle 0|\bar{q}q|0\rangle \simeq 0.4 \text{ GeV}$ , where  $G$  is an (instanton-induced) effective quark coupling constant. Note that this mass exceeds the bare quark masses by about a factor of  $\sim 100$ , being the major source of the proton mass,  $M_p \sim 3m_q^*$ , and thus of the visible mass in the Universe. Formally, the presence of the constituent quark mass (and quark condensate) is closely related to the phenomenon of ‘‘Spontaneous Breaking of Chiral Symmetry’’ (SBCS): in the limit of vanishing bare-quark masses (which is a good approximation for the very light  $u$  and  $d$  quarks), the QCD Lagrangian is invariant under rotations in isospin and chirality (handedness), i.e., transformations that change  $u$  into  $d$  quarks and left-handed into right-handed quarks. This invariance is equivalent to the conservation of isospin and chiral quantum numbers of a quark. However, the constituent quark mass breaks the chiral symmetry (i.e., massive quarks can change their chirality so that it is no longer conserved). SBCS not only manifests itself in the QCD ground-state, but also in its excitation spectrum, i.e., hadrons. Therefore, hadronic states which transform into each other under ‘‘chiral rotations’’ (so-called chiral multiplets or partners) are split in mass due to SBCS. Prominent examples in the meson spectrum are  $\pi(140)$ - $\sigma(400\text{-}1200)$  and  $\rho(770)$ - $a_1(1260)$ , or  $N(940)$ - $N^*(1535)$  in the nucleon spectrum.

In the following Section, we will discuss how the presence of strongly interacting matter affects the nonperturbative structure of the QCD vacuum and the interactions therein.

## 2.2 Strongly Interacting Matter and the QCD Phase Diagram

When heating a condensed state, the general expectation is that the condensate eventually ‘‘melts’’ (or ‘‘evaporates’’), and that the interactions are screened due to the presence of charged particles in the medium. Transferring this expectation to the QCD vacuum implies

<sup>2</sup>The origin of this force is most likely not the perturbative exchange of gluons, but nonperturbative gluon configurations - so-called instantons - which correspond to tunneling events between topologically different vacua and are characterized by a 4-dimensional ‘‘radius’’ of  $\rho \simeq (0.6 \text{ GeV})^{-1}$ , cf. Ref. [15] for a review

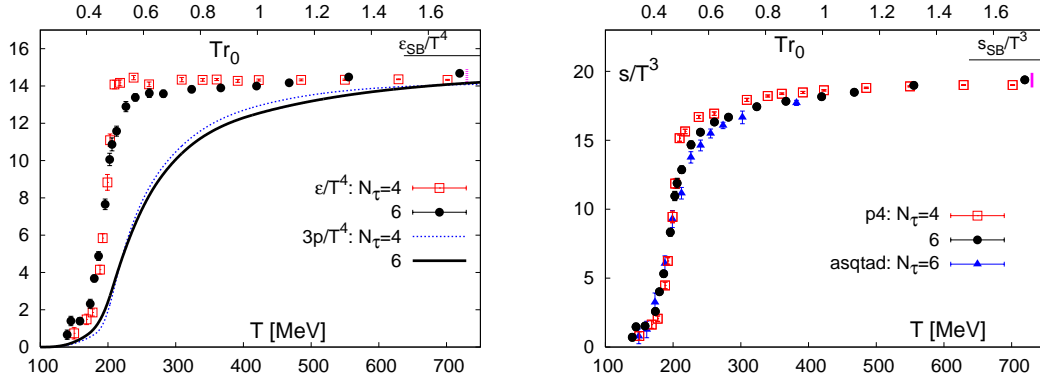


Figure 5: The equation of state of strongly interacting matter as computed in lattice QCD [12] in terms of the energy density (left panel) and entropy density (right panel) as a function of temperature (at  $\mu_B = 0$ ). The computations use bare light and strange quark masses close to their physical values.

that, at sufficiently large temperature, the condensates should vanish and the quarks and gluons are released from their hadronic bound states (deconfinement), forming the Quark-Gluon Plasma (QGP). Numerical lattice QCD (lQCD) computations of the thermodynamic partition function at finite temperature have substantially quantified this notion over the last two decades or so. The pertinent equation of state (EoS), i.e., the pressure, energy and entropy density, indeed exhibits a rather well defined transition, as shown in Fig. 5 for a lQCD calculation with close to realistic input for the bare light and strange quark masses. At high temperatures ( $T > 3T_c$ ) the equation of state is within  $\sim 15\%$  of the values expected for an ideal gas, known as the Stefan-Boltzmann (SB) limit. The SB values are given by  $\varepsilon_{q\bar{q}} = \frac{7}{8}d_{q\bar{q}}\frac{\pi^2}{30}T^4$  and  $\varepsilon_g = d_g\frac{\pi^2}{30}T^4$  with degeneracies  $d_{q\bar{q}} = N_c N_s N_{\bar{q}} N_f = 12N_f$  for quarks plus antiquarks ( $N_c=3$  for red, green and blue colors,  $N_s=2$  for spin up and down and  $N_{\bar{q}}=2$  for anti-/quarks;  $N_f$  is the number of massless flavors), and  $d_g = N_s N_c = 16$  for gluons ( $N_c=8$  color-anticolor combinations,  $N_s=2$  transverse spin polarizations); the relative factor of  $7/8$  is due to the difference of Fermi vs. Bose distribution functions for quarks vs. gluons. For  $N_f=3$  one finds  $\varepsilon_{SB} = \varepsilon_{q\bar{q}} + \varepsilon_g \simeq 15.6 T^4$ , as indicated by the “ $\varepsilon_{SB}$ ” limit in the upper right corner of the left panel in Fig. 5. Likewise, using  $P = sT - \varepsilon$  (for quark chemical potential  $\mu_q = 0$ ), one finds for the SB limit of the entropy density  $s = (10.5N_f + 16)\frac{4\pi^2}{90}T^3 \simeq 20.8 T^3$ , cf. right panel of Fig. 5.

Returning to the phase transition region, the rapid change in  $\varepsilon$  is accompanied by comparably sudden changes in the quark condensate, and the expectation value of the so-called Polyakov loop, an order parameter of deconfinement, cf. Fig. 6. The latter is, roughly speaking, proportional to the exponent of the heavy-quark free energy at large distance,  $e^{-F_{Q\bar{Q}}^\infty/T}$ , which vanishes in the confined phase (or at least becomes very small since  $F_{Q\bar{Q}}^\infty \equiv F_{Q\bar{Q}}(r \rightarrow \infty)$  is large), but is finite in the deconfined QGP.

Detailed studies of the HQ free energy as a function of the relative distance,  $r$ , of the

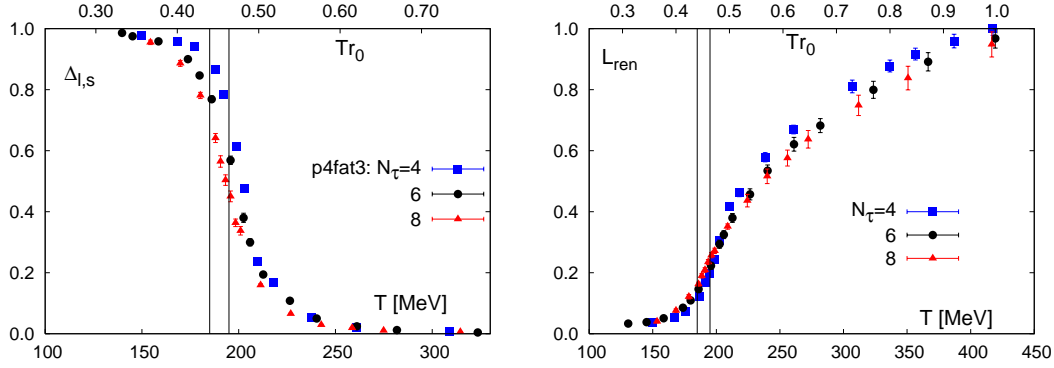


Figure 6: Lattice QCD computations of the (subtracted and normalized) light-quark chiral condensate (left panel) and the (renormalized) Polyakov loop expectation value as a function of temperature [12, 16].

$Q$ - $\bar{Q}$  pair have also been conducted in finite- $T$  lattice QCD, see, e.g., Fig. 7. One finds the qualitatively expected behavior that the interaction is increasingly screened with increasing temperature, penetrating to smaller distances, as is characteristic for a decreasing color-Debye screening length (or, equivalently, increasing Debye mass,  $\mu_D$ ). However, the implications of these in-medium modifications for the binding of quarkonium states are quite subtle. The first problem is that, unlike in the vacuum case, the identification of the free energy with an interaction potential is no longer straightforward, due to the appearance of an entropy term,  $TS_{Q\bar{Q}}$ ,

$$F_{Q\bar{Q}}(r, T) = U_{Q\bar{Q}}(r, T) - TS_{Q\bar{Q}}(r, T), \quad (4)$$

where  $U_{Q\bar{Q}}$  denotes the internal energy. It is currently an open problem whether  $F_{Q\bar{Q}}$  [18] or  $U_{Q\bar{Q}}$  [19–23] (or even a combination thereof [24]) is the most suitable quantity to be inserted into a potential model calculation for quarkonium states in the medium (typically carried out using a Schrödinger equation). The different choices lead to considerably different results for the quarkonium binding in the QGP. On the one hand, when directly using the free energy  $F_{Q\bar{Q}}$ , the charmonium ground state (the  $S$ -wave  $J/\psi$  or  $\eta_c$  states) dissolves not far above the critical temperature, at about  $1.2 T_c$  [18]. On the other hand, the use of  $U_{Q\bar{Q}}$  implies deeper potentials and thus stronger binding, and the ground-state charmonium survives up to temperatures of  $\sim 2$ - $2.5 T_c$ . The stronger bound bottomonia are more robust and may not dissolve until  $\sim 4 T_c$ .

An alternative way to address the problem of quarkonium dissociation in the QGP is the computation of  $Q$ - $\bar{Q}$  correlation functions, which are basically thermal Green’s functions (or  $Q$ - $\bar{Q}$  propagators). However, the oscillating nature of the propagator for physical energies (i.e., in real time) renders numerical IQCD evaluations intractable. However, one can apply a trick by transforming the problem into “imaginary time”, where the propagators are exponentially damped. The price one has to pay is an analytical continuation back

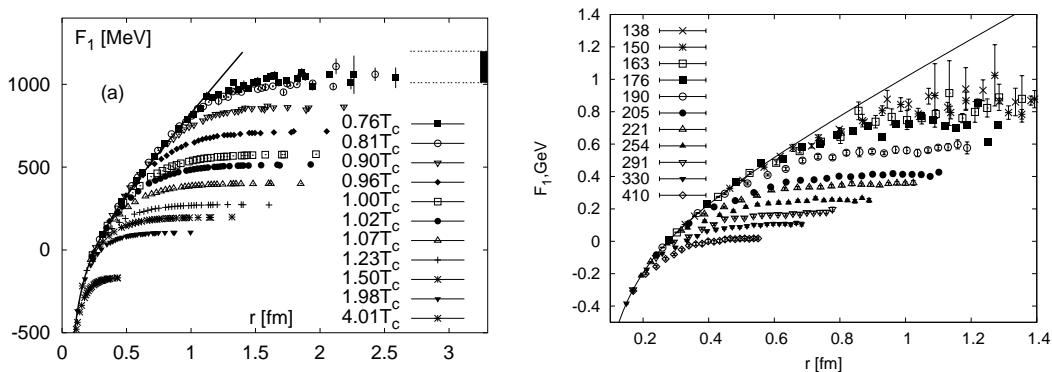


Figure 7: The heavy-quark free energy as a function of size,  $r$ , of the HQ pair, for various temperatures as computed in lattice QCD [13, 17].

into the physical (real time) regime of positive energies. This transformation is particularly problematic at finite temperature, where the imaginary-time axis in the statistical operator (free energy) is given by the inverse temperature, which severely limits the accuracy in the analytic continuation (especially for a limited discrete number of points on the imaginary-time axis). However, probabilistic methods, in particular the so-called Maximum Entropy Method (MEM), have proven valuable in remedying this problem [26]. LQCD computations of charmonium correlation functions in the QGP, followed by a MEM analysis to extract pertinent spectral functions, support the notion that the ground state ( $S$ -wave) charmonium survives up to temperatures of  $\sim 1.5-2 T_c$  [27], cf., e.g., the left panel of Fig. 8. Even in the light-quark sector IQCD computations indicate the possibility that mesonic resonance states persist above the phase transition [28, 29], as illustrated in the right panel of Fig. 8.

To summarize this section, first principle lattice-QCD calculations at finite temperature have confirmed that hadronic matter undergoes a transition into a Quark-Gluon Plasma. This transition is characterized by rapid changes in the equation of state around a temperature of  $T_c=0.15-0.20$  GeV, which is accompanied by variations in order parameters associated with deconfinement and the restoration of chiral symmetry (i.e., vanishing of the chiral quark condensate). While thermodynamic state variables are within 15% of the ideal gas limit at temperatures of  $\geq 3 T_c$ , the analysis of the heavy-quark potential and mesonic spectral functions indicate substantial nonperturbative effects at temperatures below  $\sim 2 T_c$ . This suggests that up to these temperatures the QGP is quite different from a weakly interacting gas of quarks and gluons. Substantial progress in our understanding of hot and dense QCD matter has emerged on a complementary front, namely from experiments using ultrarelativistic heavy-ion collisions. The following Section gives a short overview of the key observations and pertinent theoretical interpretations.

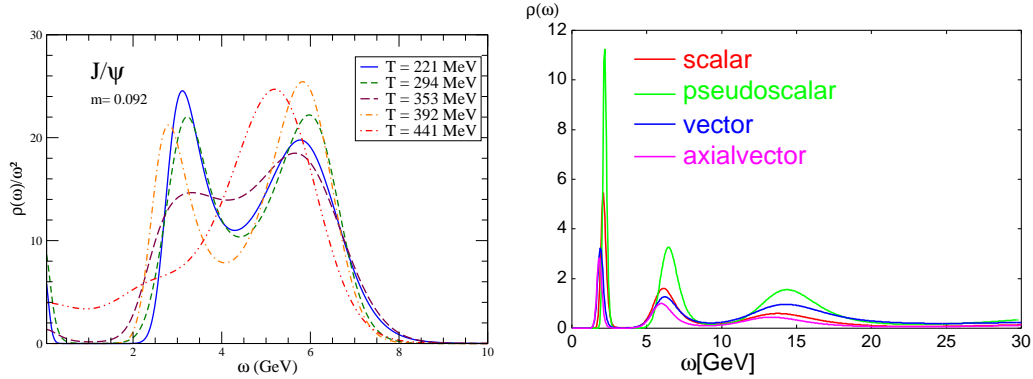


Figure 8: Meson spectral functions in the Quark-Gluon Plasma, based on imaginary-time correlation functions computed in finite- $T$  lattice QCD, followed by a transformation in the physical regime using the Maximum Entropy Method. Left panel:  $S$ -wave charm-anticharm channel (spin-parity  $J^P = 1^-$ , corresponding to the  $J/\psi$  meson) in a QGP with  $N_f = 2$  flavors [27]; the critical temperature in these calculations is about  $T_c \simeq 200$  MeV. Right panel: quark-antiquark channels with a bare quark mass corresponding to strange quarks [28], in the scalar ( $J^P = 0^+$ ), pseudoscalar ( $J^P = 0^-$ ), vector ( $J^P = 1^-$ ) and axialvector ( $J^P = 1^+$ ) channels in a pure gluon plasma at  $T=1.4 T_c$ .

### 2.3 Relativistic Heavy Ion Collisions and the Quest for the QGP

The first years of experiments at the Relativistic Heavy-Ion Collider have indeed provided convincing evidence that a thermalized medium is produced in  $\sqrt{s} = 200$  AGeV collisions. In this section we give a brief summary of the basic observations and pertinent interpretations [30]<sup>3</sup>. A schematic pictorial sketch of the main stages of the evolution of a head-on collision of heavy nuclei is displayed in Fig. 9. The main observables are momentum spectra of various hadron species. We will concentrate on particles with zero longitudinal momentum ( $p_z=0$ ) in the center-of-mass frame of a nucleus-nucleus collision, the so-called mid rapidity ( $y=0$ ) region, where one expects the largest energy deposition of the interpenetrating nuclei. The main kinematic variable is thus the transverse momentum ( $p_T$ ) of a particle. Three major findings at RHIC thus far may be classified by their  $p_T$  regime (see Fig. 10 for 3 representative measurements):

- Thermalization and collective matter expansion in the low- $p_T$  regime  $p_T \simeq 0$ -2 GeV;
- Quark coalescence in the intermediate- $p_T$  regime,  $p_T \simeq 2$ -5 GeV;
- Jet quenching in the high- $p_T$  regime,  $p_T \geq 5$  GeV.

It turns out that all of the 3 regimes, and the associated physical phenomena, are relevant for our discussion of heavy-quark observables below. In the following, we will elaborate on the characteristic features of these momentum regimes in some detail.

<sup>3</sup>For an assessment of the earlier CERN-SPS experiments at lower energies, cf. Ref. [31].

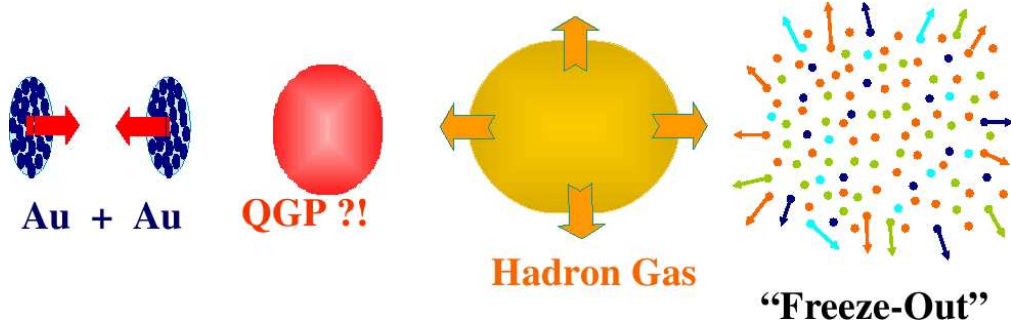


Figure 9: Schematic representation of the various stages of a heavy-ion collision. From left to right: incoming nuclei at highly relativistic energies moving at close to the speed of light (which induces a substantial Lorentz contraction relative to their transverse size; at full RHIC energy of 100+100 GeV, the Lorentz contraction is a factor of  $\sim 1/100$ ); upon initial impact of the nuclei, primordial (“hard”) nucleon-nucleon collisions occur; further reinteractions presumably induce the formation of a Quark-Gluon Plasma (after  $\tau_0 = 0.5-1$  fm/c), whose pressure drives a collective expansion and cooling (for a duration of  $\tau_{\text{QGP}} \simeq 5$  fm/c), followed by hadronization and further expansion in the hadronic phase (for a duration of  $\tau_{\text{HG}} \simeq 5 - 10$  fm/c); at thermal freezeout the (short-range) strong interactions cease (after approximately 15 fm/c total fireball lifetime).

In the low- $p_T$  regime, the spectra of the most abundantly produced hadrons ( $\pi$ ,  $K$ ,  $p$ ,  $\Lambda$ , etc.) are well described by hydrodynamic simulations of an exploding fireball [35–38]. At its breakup (or thermal freezeout), where the (short-range) interactions of the hadrons cease rather abruptly, the fireball matter is expanding at an average collective velocity of about 60% of the speed of light and has cooled down to a temperature of about  $T_{\text{fo}} \simeq 100$  MeV. The hadro-chemistry of the fireball, characterized by the thermal ratios of the various hadron species [11], is “frozen” at a higher temperature of about  $T_{\text{ch}} \simeq 170$  MeV (as represented by the “data” points in Fig. 2). The separation of chemical and thermal freezeout is naturally explained by the large difference in the inelastic and elastic reaction rates in a hadronic gas. Elastic scattering among hadrons is dominated by strong resonances (e.g.,  $\pi\pi \rightarrow \rho \rightarrow \pi\pi$  or  $\pi N \rightarrow \Delta \rightarrow \pi N$ ) with large cross sections,  $\sigma_{\text{res}} \simeq 100$  mb, implying a thermal relaxation time of about  $\tau_{\text{therm}} \simeq \langle \sigma \rho_h v_{\text{rel}} \rangle \simeq 1$  fm/c (assuming a typical hadron density of  $0.2 \text{ fm}^{-3}$  and a relative velocity of  $v_{\text{rel}} = 0.5c$ ). Inelastic cross sections, on the other hand, are typically around 1 mb, implying chemical relaxation times in a hadron gas of  $\sim 100$  fm/c, well above its lifetime of  $\sim 10$  fm/c.

A hadronic observable which is sensitive to the early expansion phases of the fireball is the elliptic flow,  $v_2$ , which characterizes the azimuthal asymmetry in the emitted hadron spectra (i.e., the second harmonic) according to

$$\frac{dN_h}{d^2p_T dy} = \frac{dN_h}{\pi dp_T^2 dy} [1 + 2v_2(p_T) \cos(2\phi) + \dots] \quad (5)$$

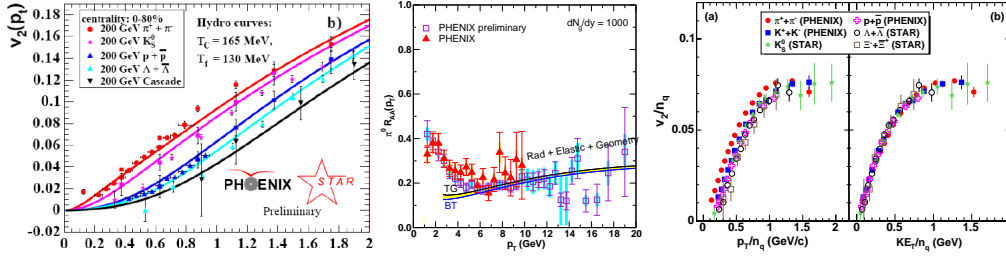


Figure 10: Key experimental measurements in Au-Au collisions at the Relativistic Heavy Ion Collider in its first years of operation, as reflected in transverse-momentum spectra of hadrons [30]. Left panel: Elliptic flow compared to hydrodynamic calculations [32] in the low- $p_T$  regime; middle panel: nuclear modification factor of neutral pions compared to perturbative jet-quenching calculations [33] in the high- $p_T$  regime; right panel: universal scaling of the hadronic  $v_2$  interpreted as an underlying quark  $v_2$  [34].

(at mid rapidity, the system is mirror symmetric in the transverse  $x$ - $y$  plane and odd Fourier components in the azimuthal angle  $\phi$  vanish). In a noncentral Au-Au collision, the initial nuclear overlap zone in the transverse plane is “almond”-shaped, cf. Fig. 11. Once the system thermalizes, the pressure gradients along the short axis of the medium are larger than along the long axis. As a result, hydrodynamic expansion will be stronger along the  $x$ -axis relative to the  $y$ -axis, and thus build up an “elliptic flow” in the collective matter expansion, which eventually reflects itself in the final hadron spectra via a positive  $v_2$  coefficient. The important point is that a large  $v_2$  can only be generated if the thermalization of the medium is rapid enough: an initial period of (almost) free streaming will reduce the spatial anisotropy and thus reduce the system’s ability to convert this spatial anisotropy into a momentum anisotropy (i.e.,  $v_2$ ). In this way, the magnitude of  $v_2$  (and its  $p_T$  dependence) is, in principle, a quantitative “barometer” of the thermalization time,  $\tau_0$ . Applications of ideal relativistic hydrodynamics have shown that the experimentally measured  $v_2(p_T)$  for various hadrons ( $\pi$ ,  $K$ ,  $p$ ,  $\Lambda$ ) is best described when implementing a thermalization time of  $\tau_0=0.5$ -1 fm/c. The agreement with data extends from  $p_T = 0$  to  $\sim 2$ -3 GeV, which (due to the exponentially falling spectra) comprises more than 95% of the produced hadrons. Not only do the interactions for thermalizing the matter rapidly have to be very strong, but, for ideal hydrodynamics to build up the observed  $v_2$ , the viscosity of the formed medium must remain very small (it is zero in ideal hydrodynamics): the typical timescale for build-up of the observed  $v_2$  is on the order of the system size or QGP lifetime,  $\tau_{\text{QGP}} \simeq 5$  fm/c. These features have triggered the notion of a “strongly-coupled” QGP (sQGP); its initial energy density at RHIC, as implied by the above thermalization times, amounts to  $\varepsilon_0 \simeq 10$ -20 GeV/fm<sup>3</sup>, which is a factor of  $\sim 10$  above the estimated critical energy density for the phase transition (and a factor of  $\sim 100$  above that for normal nuclear matter).

In the high- $p_T$  regime, the production mechanism of hadrons changes and becomes computable in perturbative QCD, in terms of hard parton-parton collisions upon first im-



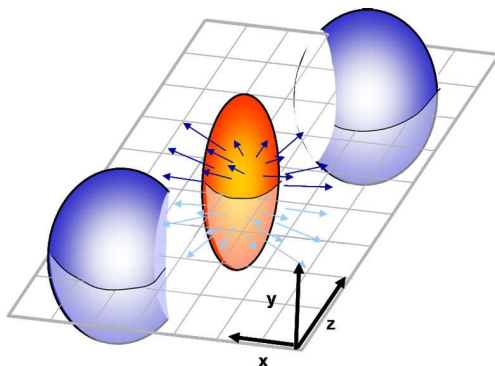


Figure 11: Schematic representation of a noncentral heavy-ion collision, characterized by an almond-shaped initial overlap zone, and a subsequent pressure-driven build-up of elliptic flow.

part of the incoming nucleons (cf. left panel in Fig. 9). The produced high-energy partons subsequently fragment into a (rather collimated) spray of hadrons, called jet. Back-to-back jets are routinely observed in high-energy collisions of elementary particles, but are difficult to identify in the high-multiplicity environment of a heavy-ion collision. However, a jet typically contains a “leading” particle which carries most of the momentum of the parent parton (as described by an empirical “fragmentation” function). High- $p_T$  spectra in heavy-ion collisions thus essentially determine the modification underlying the production of the leading hadron in a jet. This modification is quantified via the “nuclear modification factor”,

$$R_{AA}(p_T) = \frac{dN_h^{AA}/dp_T}{N_{\text{coll}} dN_h^{NN}/dp_T}, \quad (6)$$

where the numerator denotes the hadron spectrum in the nucleus-nucleus collision and the denominator represents the spectrum in an elementary nucleon-nucleon collision, weighted with the number of binary  $N$ - $N$  collisions in the primordial stage of the  $A$ - $A$  collision. Thus, if there is no modification of the leading hadron spectrum in the heavy-ion collision, then  $R_{AA}(p_T \geq 5 \text{ GeV}) = 1$ . RHIC data on  $\pi$  production in central Au-Au collisions have found a large suppression by a factor of 4-5 up to  $p_T \simeq 20 \text{ GeV}$ . Originally, this has been attributed to radiative energy-loss, i.e., induced gluon radiation off a high-energy quark (or gluon) traversing a gluon plasma [39, 40], as computed within perturbative QCD (pQCD). In the approach of Ref. [39], the initially extracted gluon densities turned out to be consistent with those inferred from hydrodynamic calculations in the low- $p_T$  regime. In the approach of Ref. [40], the interaction strength of the energy-loss process is quantified via the transport coefficient  $\hat{q} = Q^2/\lambda$ , which characterizes the (squared) momentum transfer per mean free path of the fast parton; the experimentally observed suppression requires this quantity to take on values of 5-15  $\text{GeV}^2/\text{fm}$ , which is several times larger than expected in pQCD [41]. More recently, the importance of elastic energy loss has been realized, in particular in the context of heavy-quark propagation [33, 42–45], as we will discuss in more

detail below.

In the intermediate- $p_T$  regime, RHIC experiments have observed an unexpectedly large ratio of baryons to mesons, e.g.,  $p/\pi \simeq 1$  or  $(\Lambda + \bar{\Lambda})/(4K_s^0) \simeq 1.3$  in central Au-Au collisions. On the one hand, within the pQCD energy loss picture, the typical value of  $p/\pi$  is close to  $\sim 0.2$  as observed in elementary  $p$ - $p$  collisions. On the other hand, within hydrodynamic calculations, a collective flow could, in principle, account for such an effect, but the applicability of hydrodynamics appears to cease at momenta of  $p_T \geq 3$  GeV (as, e.g., indicated by the saturation (leveling off) of the elliptic flow, which in hydrodynamics continues to grow). Another remarkable observation in intermediate- $p_T$  hadron spectra is a constituent-quark number scaling (CQNS) of the hadronic  $v_{2,h}(p_T)$ , as determined by the number,  $n$ , of constituent quarks in each hadron,  $h$ , giving rise to a single, universal function,

$$v_{2,q}(p_T/n) = v_{2,h}(p_T)/n, \quad (7)$$

which is interpreted as the partonic (quark)  $v_2$  at the time of hadronization. Both CQNS and the large baryon-to-meson ratios are naturally explained in terms of quark coalescence processes of a collectively expanding partonic source at the phase transition [46–48]. The most recent experimental data [34, 49] indicate that the scaling persists at a surprisingly accurate level even at low  $p_T$ , but only when applied as a function of the transverse kinetic energy,  $\text{KE}_T = m_T - m_h$ , of the hadrons (where  $m_T = (p_T^2 + m_h^2)^{1/2}$  is the total transverse energy of the hadron, and  $m_h$  its rest mass). In Ref. [50], the quark coalescence model has been reformulated utilizing a Boltzmann transport equation where the hadron formation process is realized via the formation of mesonic resonances close to  $T_c$ . This approach overcomes the instantaneous approximation of previous models, ensuring energy conservation in the coalescence process, as well as the proper thermodynamic equilibrium limit. This, in particular, allows for an extension of the coalescence idea into the low- $p_T$  regime, and initial calculations are consistent with  $\text{KE}_T$  scaling for  $v_{2,h}$ .

To summarize this section, we conclude that RHIC data have provided clear evidence for the formation of an equilibrated medium with very small viscosity (an almost “perfect liquid”) and large opacity with associated energy densities well above the critical one; in addition, indications for the presence of partonic degrees of freedom have been observed. This medium has been named the strongly coupled QGP, or sQGP. However, the understanding of its microscopic properties remains an open issue at this point: What are the relevant degrees of freedom and their interactions around and above  $T_c$ ? Are the 3 main phenomena described above related, and, if so, how? Is there direct evidence for deconfinement and/or chiral symmetry restoration? Results from lattice QCD, as discussed in the previous section, may already have provided several important hints, but tighter connections to RHIC data need to be established.

Toward this goal, heavy-quark observables are hoped to provide new decisive and quantitative insights: Do charm and bottom quarks participate in the flow of the medium, despite their large mass? Do they even thermalize at low  $p_T$ ? Do they suffer jet quenching at high  $p_T$ ? Do they corroborate evidence for quark coalescence processes? Initial measurements of heavy-quark observables have been performed providing tantalizing evidence that the

answer to these questions may indeed be largely positive: a substantial elliptic flow and suppression of single-electron spectra associated with semileptonic heavy-meson decays has been observed, i.e., electrons (and positrons) arising via decays of the type  $D \rightarrow e\nu X$  and  $B \rightarrow e\nu X$  (the heavy-light mesons,  $D = (c\bar{q})$  and  $B = (b\bar{q})$ , are composed of a heavy quark ( $c, b$ ) and a light antiquark ( $\bar{q} = \bar{u}, \bar{d}$ ), and as such are the main carriers of heavy quarks in the system).

We now turn to the main subject of this article, i.e., the theoretical and phenomenological description of heavy-quark interactions in the QGP and pertinent observables at RHIC.

### 3 Heavy Quarks in the Quark-Gluon Plasma

The special role of heavy quarks ( $Q = b, c$ ) as a probe of the medium created in heavy-ion collisions resides on the fact that their mass is significantly larger than the typically attained ambient temperatures or other nonperturbative scales,  $m_Q \gg T_c, \Lambda_{\text{QCD}}$ .<sup>4</sup> This has several implications:

- (i) The production of heavy quarks is essentially constrained to the early, primordial stages of a heavy-ion collision. Thus the knowledge of the initial heavy-quark (HQ) spectrum (from, say,  $p$ - $p$  collisions) can serve as a well defined initial state, even for low-momentum heavy quarks. The latter feature renders heavy-quark observables a prime tool to extract transport properties of the medium.
- (ii) Thermalization of heavy quarks is “delayed” relative to light quarks by a factor of  $\sim m_Q/T \simeq 5$ -15. While the bulk thermalization time is of order  $\sim 0.5$  fm/ $c$ , the thermal relaxation of heavy quarks is expected to occur on a timescale comparable to the lifetime of the QGP at RHIC,  $\tau_{\text{QGP}} \simeq 5$  fm/ $c$ . Based on the thus far inferred properties of the sQGP, charm quarks could “thermalize” to a certain extent, but not fully. Therefore, their spectra should be significantly modified, but still retain memory about their interaction history – an “optimal” probe. According to this estimate, bottom quarks are expected to exhibit notably less modification.
- (iii) As is well-known from electrodynamics, Bremsstrahlung off an accelerated (or decelerated) charged particle is suppressed by a large power of its the mass,  $\sim (m_q/m_c)^4$  for heavy relative to light quarks. Therefore, induced gluon radiation off heavy quarks (i.e., radiative energy loss) is much suppressed relative to elastic scattering.
- (iv) The typical momentum transfer from a thermal medium to a heavy quark is small compared to the HQ momentum,  $p_{\text{th}}^2 \sim m_Q T \gg T^2$  (where  $p_{\text{th}}$  is the thermal momentum of a heavy quark in nonrelativistic approximation,  $p_{\text{th}}^2/2m_Q \simeq 3 T/2$ ; for a relativistically moving quark, it is parametrically even larger,  $p_{\text{th}} \sim m_Q v$ ). This renders a Brownian Motion approach (Fokker-Planck equation) a suitable and

---

<sup>4</sup>Note that the production of the heaviest known quark, the top, is out of reach at RHIC; moreover, its lifetime,  $\tau_t = 1/\Gamma_t \simeq 0.1$  fm/ $c$ , is by far too short to render it a useful probe.

controlled theoretical framework for describing the diffusion of a heavy quark in the (s)QGP.

- (v) The HQ mass can furthermore be utilized as a large scale in developing effective (nonperturbative) interactions, such as HQ effective theory or potential model approaches. In principle, this allows to make contact with static interaction potentials from finite-temperature lattice QCD, although a number of issues have to be resolved before reliable quantitative predictions can be made.
- (vi) At low momenta, nonperturbative (resummation) effects become relatively more important with increasing mass. E.g., for bound state formation, the binding energy is known to increase with the (reduced) mass of the constituents. For the concrete problem of the charm diffusion constant, it has recently been shown that the perturbation series is badly convergent even for values of the strong coupling constant as small as  $\alpha_s = 0.1$  [51].

Before first RHIC data on HQ observables became available, the expectation based on pQCD radiative energy loss was that the  $D$ -meson spectra are much less suppressed than light hadron spectra [52], with a small elliptic flow of up to  $v_2^D \simeq 4\%$  [53]. At the same time, the importance of elastic collisions was emphasized in Refs. [42–44]. In particular, in Ref. [42] nonperturbative HQ resonance interactions in the QGP (motivated by lattice QCD results, cf. Fig. 8) were introduced and found to reduce the HQ thermalization times by a factor of  $\sim 3$  compared to elastic pQCD scattering. Predictions for the  $D$ -meson  $v_2$  and  $p_T$  spectra in the limiting case in which the degree of HQ thermalization is similar to light quarks can be found in Ref. [54]; including the effects of coalescence with light quarks, the  $D$ -meson elliptic flow reaches up to around  $v_2^D \simeq 15\%$ , about a factor of  $\sim 4$  larger than in the pQCD energy-loss calculations. This analysis also demonstrated the important feature that the single-electron ( $e^\pm$ ) spectra arising from the semileptonic decays,  $D \rightarrow e\nu X$ , closely trace the suppression ( $R_{AA}$ ) and elliptic flow of the parent  $D$  meson (see also Ref. [55]). In the following, we elaborate on the underlying approaches and further developments with applications to HQ transport properties and RHIC data.

### 3.1 Heavy-Quark Interactions in the QGP

The scattering of charm and bottom quarks in a Quark-Gluon Plasma is dominated by interactions with the most abundant particles in the medium, i.e., gluons as well as light ( $u$  and  $d$ ) and strange quarks. The basic quantity to be evaluated is therefore the scattering matrix (or cross section), which can be further utilized to compute in-medium HQ self-energies and transport coefficients. For reasons given in the previous Section we focus on elastic  $2 \rightarrow 2$  scattering processes,  $Q + i \rightarrow Q + i$  with  $i = g, u, d, s$ . Our discussion is organized into perturbative (Sec. 3.1.1) and nonperturbative approaches (Secs. 3.1.2 and 3.1.3). While the effective resonance model (Sec. 3.1.2) involves a priori undetermined parameters in terms of the resonance masses and coupling constants, the lattice-QCD based potential

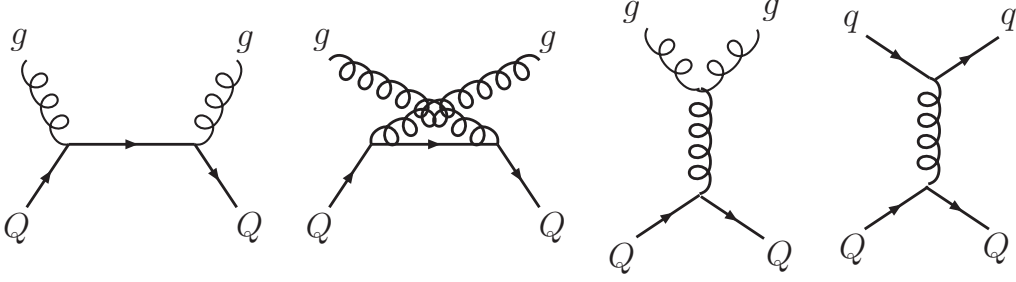


Figure 12: Feynman diagrams for leading-order perturbative HQ scattering off light partons.

scattering (Sec. 3.1.3) is an attempt to generate the heavy-light quark interactions microscopically without free parameters (albeit with significant uncertainties in the extraction of the interaction potentials).

### 3.1.1 Perturbative Scattering

In QCD, the simplest possible diagrams for HQ interactions with light partons are given by leading order (LO) perturbation theory. The pertinent Feynman diagrams are very similar to the ones depicted in Fig. 3, and are summarized in Fig. 12. As discussed in Sec. 2.1, these processes can be expected to constitute a realistic description of HQ scattering in regimes where the strong coupling constant,  $\alpha_s$ , is small (higher order diagrams will contribute with higher powers in  $\alpha_s$ ). In principle, this can be realized either for large HQ momenta (implying the relevant momentum transfers to be large) or at high temperatures where the interaction is screened and/or the typical momentum transfer of order  $Q^2 \sim T^2$  is large. Since the color charge of gluons is larger than that of quarks (by a factor of 9/4 to order  $\alpha_s$ ), the dominant contribution to pQCD scattering arises from interactions with gluons, more precisely the  $t$ -channel gluon exchange in  $Q(p_1^{(4)}) + g(p_2^{(4)}) \rightarrow Q(p_3^{(4)}) + g(p_4^{(4)})$ , where  $p_i^{(4)} = (E_i, \vec{p}_i)$  denotes the energy-momentum vector (or 4-momentum) of particle  $i$  (we use  $p_i = |\vec{p}_i|$  for the magnitude of the 3-momentum). The corresponding differential cross section is given by

$$\frac{d\sigma_{gQ}}{dt} = \frac{1}{16\pi(s - M^2)^2} \overline{|\mathcal{M}|^2}, \quad (8)$$

where  $t = (p_3^{(4)} - p_1^{(4)})^2 = 2(m_Q^2 - E_1 E_2 + \vec{p}_1 \cdot \vec{p}_3)$  is the energy-momentum transfer on the heavy quark with  $\vec{p}_1 \cdot \vec{p}_3 = p_1 p_3 \cos \Theta$ ,  $s$  is the squared center-of-mass energy  $s = (p_1^{(4)} + p_2^{(4)})^2$ , and  $\Theta$  the scattering angle of the heavy quark. The squared scattering amplitude, averaged over initial and summed over final spin polarizations,

$$\overline{|\mathcal{M}|^2} = \pi^2 \alpha_s^2 \left[ \frac{32(s - M^2)(s + t - M^2)}{t^2} + \dots \right], \quad (9)$$

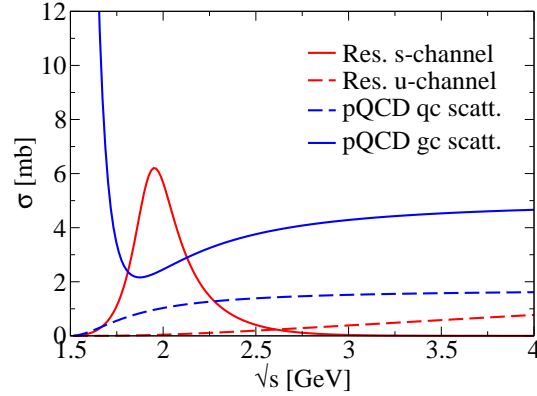


Figure 13: Total HQ scattering cross sections off light partons in pQCD (blue lines) and within the effective resonance model (red lines) [56].

turns out to be dominated by the  $t$ -channel gluon exchange diagram (third panel in Fig. 12), corresponding to the expression explicitly written in the brackets. The factor  $1/t^2$  represents the (squared) propagator of the exchanged gluon which leads to a large cross section for small  $t$  implying a small scattering angle  $\Theta$ , i.e., forward scattering. However, as discussed in Sec. 2.2, the interaction is screened in the medium which, in a simplistic form, can be implemented as an in-medium gluon propagator  $1/(t - \mu_D^2)$ , leading to a reduction of the cross section (note that for  $t$ -channel gluon exchange, the 4-momentum transfer,  $t$ , is negative). To lowest order in perturbation theory, the gluon Debye mass is given by  $\mu_D \sim gT$ . The total cross section follows from integrating the expression in Eq. (8) over  $t$ ; the results including all LO diagrams for charm-quark scattering off quarks and gluons are displayed in Fig. 13. The total pQCD cross sections, computed for an optimistically large  $\alpha_s = 0.4$ , are, in fact, quite sizable, at around  $\sigma_{\text{tot}} = 4(1.5)$  mb for gluons (quarks). In a schematic estimate these cross sections may be converted into a reaction rate by using the “pocket formula”  $\Gamma_c = \sigma_{ci} n_i v_{\text{rel}}$ . To obtain an upper limit, one may use ideal-gas massless parton densities,  $n_i = d_i \pi^2 T^3$ , with quark, antiquark and gluon degeneracies of  $d_{q\bar{q}} = 10.5 N_f$  with  $N_f = 2.5$  and  $d_g = 16$  (recall Sec. 2.2 and Fig. 5), in connection with a relative velocity  $v_{\text{rel}} = c$ . One finds  $\Gamma_c \simeq 0.4 \text{ GeV} = (0.5 \text{ fm}/c)^{-1}$ , a rather large elastic scattering rate. However, as we will see below, the relevant quantity for determining the thermalization time scale is the transport cross section, which involves an extra angular weight proportional to  $\sin^2 \Theta$  when integrating over the differential cross section. This renders pQCD scattering rather ineffective in isotropizing HQ distributions, due to its predominantly forward scattering angles; the resulting thermal relaxation times,  $\tau_Q^{\text{therm}}$ , are therefore much larger than what one would naively expect from the large scattering rate estimated above.

### 3.1.2 Resonance Model

As was discussed in Sec. 2.2, lattice calculations suggest the existence of hadronic resonances (or bound states) in the QGP for temperatures of 1-2  $T_c$ . In Ref. [42] the idea has been introduced that such resonances are present in the heavy-light quark sector and are operative in a significant increase of the interaction strength of heavy quarks in the QGP. The starting point of this investigation is an effective Lagrangian, *assuming* the presence of heavy-light fields,  $\Phi$ , which couple to a heavy quark and light antiquark according to

$$\mathcal{L}_{\Phi Qq} = \mathcal{L}_{\Phi}^0 + \mathcal{L}_Q^0 + \mathcal{L}_q^0 + \sum_m G_m Q \frac{1+\not{\psi}}{2} \Phi_m \Gamma_m \bar{q} + \text{h.c.} . \quad (10)$$

The first 3 terms on the right-hand-side represent the kinetic energy and mass terms giving rise to free particle propagation while the last term (h.c. = hermitean conjugate), roughly speaking, indicates all terms with particles and antiparticles interchanged (i.e.,  $Q \rightarrow \bar{Q}$ ,  $\bar{q} \rightarrow q$ , etc.). The key term is the explicitly written interaction term generating  $\Phi$ - $Q$ - $\bar{q}$  (3-point) vertices whose strength is controlled by pertinent coupling constants,  $G_m$ , which in this approach are free parameters. The summation over  $m$  accounts for the different quantum numbers of the  $\Phi$ -fields (which in turn are related to the structure of the coupling matrices,  $\Gamma_m$ ). The couplings can be largely inferred from symmetry considerations. As alluded to toward the end of Sec. 2.1, the spontaneous breaking of chiral symmetry (SBSC) in the vacuum implies hadronic chiral partners to split in mass; in the  $D$ -meson sector, this applies to the chiral partners in the scalar ( $J^P = 0^+$ ) - pseudoscalar ( $J^P = 0^-$ ) multiplet,  $D$  and  $D_0^*$ , as well as to the vector ( $J^P = 1^-$ ) and axialvector ( $J^P = 1^+$ ) chiral multiplet,  $D^*$  and  $D_1$ . The pertinent chiral breaking is nicely borne out of recent measurements of the  $D$ -meson spectrum in vacuum [57], where the chiral splitting has been established to amount to about  $\Delta M = 0.4$  GeV, cf. Fig. 14. In the QGP, however, the spontaneously broken chiral symmetry will be restored, recall, e.g., the left panel in Fig. 6. Chiral restoration is necessarily accompanied by the degeneracy of chiral partners, as is indeed observed in IQCD computations of meson spectral functions above  $T_c$ , cf. right panel of Fig. 8. We thus infer that the chiral partners in the  $D$ -meson spectrum, i.e., scalar and pseudoscalar (as well as vector and axialvector) should have the same mass and width in the QGP.

In addition, QCD possesses heavy-quark symmetries, in particular a spin symmetry which states that hadrons containing heavy quarks are degenerate if the HQ spin is flipped inside the hadron. Within the constituent quark model, one therefore expects a degeneracy of pseudoscalar and vector mesons, where the heavy and light quark are coupled in a relative  $S$ -wave (orbital angular momentum  $l = 0$ ) and the total spin,  $J$ , of the meson is solely determined by the coupling of the two quark spins. The asserted symmetry is accurate within  $\sim 0.1$ - $0.15$  GeV in the  $D$ -meson spectrum ( $D$ - $D^*$  and  $D_0^*$ - $D_1^*$ , cf. Fig. 14), and within  $\sim 0.05$  GeV in the  $B$ -meson spectrum (as given by the  $B(5280)$ - $B^*(5325)$  mass difference; note that the accuracy of the HQ symmetry indeed appears to scale with the inverse HQ mass,  $m_c/m_b \simeq 1/3$ ). Since the heavy-light resonance mass in the QGP itself is subject to uncertainties on the order of possibly up to a few hundred MeV, there is little point in accounting for the relatively small violations of HQ spin symmetry. In Ref. [42]

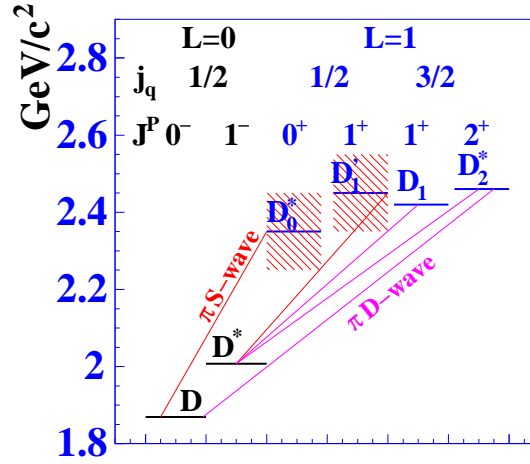


Figure 14: Level spectrum of  $D$ -mesons,  $D = (c\bar{q})$ , in the vacuum according to recent measurements reported in Ref. [57]. The masses of the states are shown as a function of their quantum numbers indicated in the upper portion of the figure. Note, on the one hand, the splitting (non-degeneracy) of the chiral partners  $D$  and  $D_0^*$ , as well as of  $D^*$  and  $D_1$ , by about  $\Delta M = 0.4$  GeV (believed to be a consequence of spontaneous breaking of chiral symmetry in the vacuum). On the other hand, HQ symmetry, implying degeneracy of  $D$ - $D^*$  and of  $D_0^*$ - $D_1$ , is satisfied within  $\Delta M = 0.15$  GeV.

it was therefore assumed that also the pseudoscalar-vector (as well as scalar-axialvector) states are degenerate.

With both chiral and HQ symmetry, the effective Lagrangian, Eq. (10), essentially contains 2 parameters in both the charm and bottom sector, which are the (universal) resonance mass,  $m_{D,B}$ , and coupling constant,  $G_{D,B}$ . The former has been varied over a rather broad window above the  $Q$ - $\bar{q}$  threshold. Note that bound states cannot be accessed in two-body scattering due to energy conservation, i.e., the bound state mass is by definition below the 2-particle threshold,  $E_{\text{thr}} = m_Q + m_{\bar{q}}$ . Once the mass is fixed, the (energy-dependent) width for the two-body decay of the resonance,  $\Phi \rightarrow Q + \bar{q}$ , is determined by the coupling constant as

$$\Gamma_{\Phi}(M) = \frac{3G_{\Phi}^2}{8\pi} \frac{(M^2 - m_Q^2)^2}{M^3} \Theta(M - m_Q), \quad (11)$$

where the mass of the light antiquark has been put to zero. To determine the coupling constant, some guidance can be obtained from effective quark models at finite temperature [58,59], where an in-medium  $D$ -meson width of several hundred MeV was found (see also Ref. [60] and Fig. 18 below).

The effective Lagrangian, Eq. (10), generates 2 diagrams for resonance exchange in heavy-light quark scattering, so-called  $s$ - and  $u$ -channels, as shown in Fig. 15. The pertinent total cross sections for charm-quark scattering are displayed by the red lines in Fig. 13,



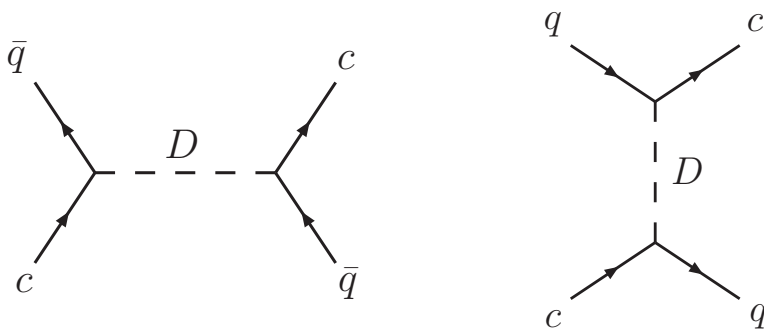


Figure 15: Feynman diagrams for nonperturbative charm-quark interactions via effective  $D$ -meson exchange in  $s$ -channel scattering off antiquarks (left panel) and  $u$  channel scattering off quarks (right panel) [42].

assuming  $D$ -meson masses and widths of  $m_D = 2$  GeV and  $\Gamma_D = 0.4$  GeV (the charm- and bottom-quark masses have been set to  $m_{c,b} = 1.5, 4.5$  GeV). In the energy regime relevant for scattering of thermal partons in the QGP,  $E_{\text{cm}} \simeq m_Q + E_q^{\text{th}} \simeq 2.2$  GeV ( $E_q^{\text{th}} \simeq 3T \simeq 0.75$  GeV at  $T = 0.25$  GeV), the cross section is largely dominated by the  $s$ -channel resonance formation, and is substantially larger than the LO pQCD result for  $Q$ - $q$  scattering. This is not so compared to pQCD scattering off gluons. However, the angular distribution of the differential  $s$ -channel resonance cross section (not shown) is essentially isotropic (in the rest system of the resonance), which renders it significantly more efficient for thermalizing the HQ distributions (as we will see in Sec. 3.2 below). The interaction introduced via the Lagrangian, Eq. (10), cannot predict at what temperatures the effective resonance fields dissolve. This, however, can be overcome if the interaction underlying the resonance formation is treated on a more microscopic level. Even more importantly, a microscopic treatment could, in principle, eliminate the coupling-constant and mass parameters. First steps in this direction will be discussed in the next section.

### 3.1.3 Potential Scattering Based on Lattice QCD

The advances in finite-temperature lQCD to compute the in-medium free energy of a  $Q$ - $\bar{Q}$  pair as a function of its size have, in principle, opened the possibility to extract their static (chromo-electric) interaction potential, see the discussion around Eq. (4). If this problem can be well defined and solved, the next desirable step is to check the quantitative consequences of such an interaction in the light quark sector (where lQCD has also found indications for resonance formation), eventually including transport and bulk properties. In Refs. [19, 61] a relativistic correction has been suggested in terms of a velocity-velocity interaction (known as the Breit interaction in electrodynamics). In those works the focus has been on the bound state problem, by solving an underlying Schrödinger equation. In Ref. [20], a  $T$ -matrix approach to the  $q$ - $\bar{q}$  interaction has been set up, which allows for a simultaneous treatment of bound and scattering states. This framework has been applied

for heavy-light quark scattering in Ref. [60]. Thus far the discussion was constrained to the color neutral (singlet)  $Q\bar{q}$  channel (i.e., a blue-antiblue, green-antigreen or red-antired color-charge combination), but a quark and an antiquark can also combine into a color-octet (a combination of red-antiblue, blue-antigreen etc.). In addition, one can extend the approach to the diquark ( $Qq$ ) channel, where color-antitriplet and sextet combinations are possible (see also Ref. [19]). Finite-temperature lattice computations of the free energy of a heavy diquark [62] suggest that the relative interaction strength in the meson and diquark systems follows the expectations of perturbative QCD (so-called Casimir scaling, which essentially reflects the color-charges of the partons), namely  $V_{Q\bar{Q}}^{(1)} = 2V_{QQ}^{(\bar{3})} = -4V_{QQ}^{(6)}$ ; that is, the interaction in the color-triplet diquark channel is half as attractive as in the color-neutral diquark channel while it is weakly repulsive for a color-sextet diquark.

The starting point for the calculations of the heavy-light quark  $T$ -matrix is the relativistic Bethe-Salpeter equation for elastic  $1 + 2 \rightarrow 3 + 4$  scattering,

$$T_m(1, 2; 3, 4) = K_m(1, 2, 3, 4) + \int \frac{d^4k}{(2\pi)^4} K_m(1, 2; 5, 6) G^{(2)}(5, 6) T_m(5, 6; 3, 4), \quad (12)$$

which accounts for the full 4-dimensional energy-momentum dependence of the scattering process (including “off-shell” particles for which energy and 3-momentum are independent variables);  $m$  characterizes all quantum numbers of the composite meson or diquark (color, total spin and flavor),  $K_m$  is the interaction kernel and  $G^{(2)}(5, 6)$  is the two-particle propagator in the intermediate state of the scattering process. The integration in the second term of Eq. (12) accounts for all possible momentum transfers in compliance with energy-momentum conservation. The labels  $j = 1, \dots, 6$  denote the quantum numbers (including 4-momentum) of the scattered single particles. Eq. (12) represents a rather involved integral equation for the full scattering  $T$ -matrix. However, the (static) potentials extracted from lQCD do not contain the rich information required for the 4-D interaction kernel  $K_m$ . It is therefore in order to adopt suitable reduction schemes [63, 64], which are well-known in nuclear physics, e.g., in the context of nucleon-nucleon scattering [65]. A reduction amounts to neglecting additional particle-antiparticle fluctuations for the intermediate 2-particle propagator and puts the latter on the energy shell, which allows one to perform the energy integration (over  $k_0$ ) in Eq. (12). Importantly, it furthermore enables to identify the reduced interaction kernel with a 2-body potential,  $V_m$ , and therefore to establish the connection to the potentials extracted from lattice QCD. The now 3-dimensional scattering equation, known as Lippmann-Schwinger (LS) equation, is amenable to an expansion in partial waves characterized by the angular momentum quantum number,  $l = 0, 1, \dots$ , corresponding to relative  $S$ - and  $P$ -waves, etc. Assuming HQ spin symmetry, the spin quantum number does not explicitly enter, and one arrives at

$$T_{a,l}(E; p', p) = V_{a,l}(p', p) + \frac{2}{\pi} \int dk k^2 V_{a,l}(p', k) G_{Qq}(E; k) T_{a,l}(E; k, p), \quad (13)$$

where  $a = 1, \bar{3}, 6, 8$  labels the color channel. In the Thompson reduction scheme, the

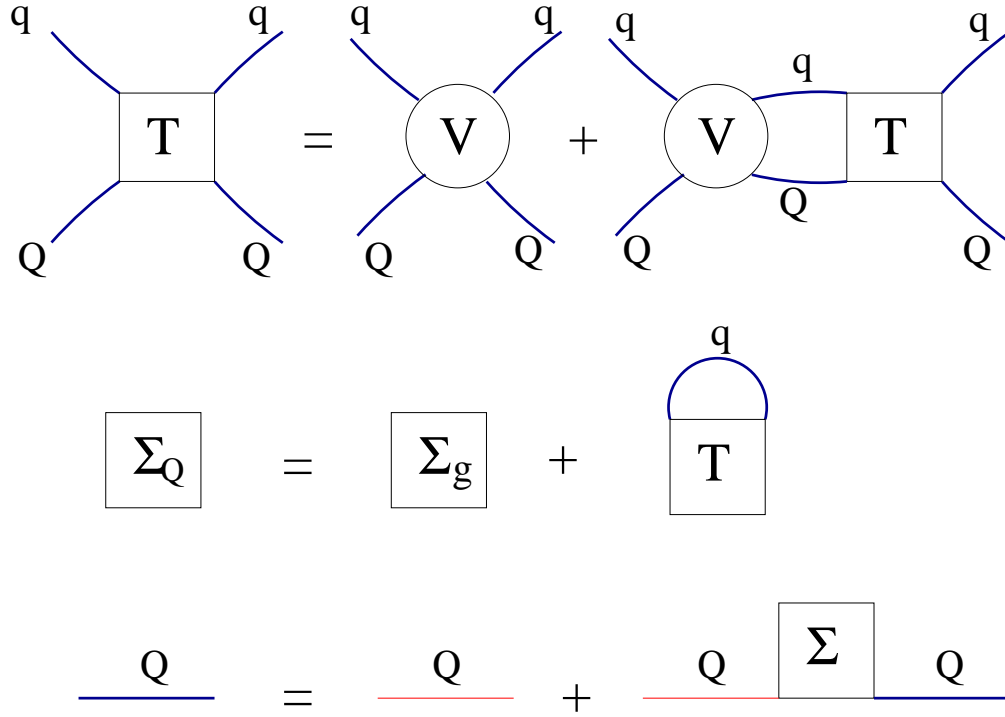


Figure 16: Diagrammatic representation of the Brueckner problem for HQ interactions in the QGP [60,66]; upper panel:  $T$ -matrix equation for HQ scattering off thermal light quarks or antiquarks; middle panel: HQ self-energy due to interactions with gluons and quarks or antiquarks; lower panel: Dyson equation for the in-medium HQ propagator.

intermediate heavy-light quark-quark (or quark-antiquark) propagator takes the form

$$G_{Qq}(E; k) = \frac{1}{4} \frac{1 - f(\omega_k^Q) - f(\omega_k^q)}{E - (\omega_k^q + i\Sigma_I^q(\omega_k^q, k)) - (\omega_k^Q + i\Sigma_I^Q(\omega_k^Q, k))} \quad (14)$$

with  $\omega_k^{q,Q} = (m_{q,Q}^2 + k^2)^{1/2}$  the on-shell quark energies, and  $f(\omega_k^{q,Q})$  the thermal Fermi distribution functions (the numerator in Eq. (14) accounts for Pauli blocking, which, however, is essentially irrelevant at the temperatures considered here). A pictorial representation of the  $T$ -matrix scattering equation is given in the upper panel of Fig. 16. Due to the interactions with the medium, the quark propagators themselves are modified which is encoded in a single-quark self-energy,  $\Sigma_{q,Q}$ , figuring into the 2-particle propagator, Eq. (14). It can be related to the heavy-light  $T$ -matrix, as well as due to interactions with gluons, as

$$\Sigma_Q(k; T) = \Sigma_{Qg} + \int \frac{d^3p}{2\omega_p^q} f(\omega_p^q) T_{Qq}(E; p, k), \quad (15)$$

cf. the middle panel in Fig. 16. The self-energy can be resummed in a Dyson equation for

the single-quark propagator according to

$$D_Q = D_Q^0 + D_Q^0 \Sigma_Q D_Q, \quad (16)$$

where the free propagator is given by  $D_Q^0(\omega, k) = 1/(\omega - \omega_k^0)$  (omitting any quantum number structure and denoting the free particle on-shell energy by  $\omega_k^0$ ). The Dyson equation is graphically displayed in the lower panel of Fig. 16. It can be solved algebraically, resulting in the full in-medium single-particle propagator

$$D_Q = \frac{1}{\omega - \omega_k^0 - \Sigma_Q}. \quad (17)$$

The convolution of the full propagators,  $D_q$  and  $D_Q$ , within the Thompson reduction scheme leads to the 2-particle propagator, Eq. (14). In general, the self-energy is a complex-valued quantity (as is the  $T$ -matrix), with its real part affecting the in-medium quasiparticle mass while the imaginary part characterizes the attenuation (absorption) of the propagating particle (wave).

Since the HQ self-energy depends on the heavy-light  $T$ -matrix, and the latter, in turn, depends on the self-energy, one is facing a Brueckner-type self-consistency problem, as illustrated in Fig. 16. In the light-quark sector, the system of Eqs. (13) and (15) has been solved by numerical iteration and moderate effects due to self-consistency have been found. For a heavy quark, the impact of self-consistency (which to a large extent is governed by the real parts of  $\Sigma$ ) is weaker (since the relative corrections to the HQ mass are not as large as for light quarks). Therefore, in the calculations of the  $T$ -matrix in Ref. [60], the real and imaginary parts of the self-energies of light and heavy quarks have been approximated by (constant) thermal mass corrections (largely being attributed to the gluon-induced self-energy term,  $\Sigma_{Qg}$ , in Eq. (15) and resulting in  $m_q^{\text{th}} = 0.25$  GeV and  $m_{c,b}^{\text{th}} = 1.5, 4.5$  GeV) and quasiparticle widths of  $\Gamma_{Q,q} = 0.2$  GeV. The underlying heavy-light interaction potentials,  $V_{1,\bar{3},6,8}$ , have been identified with the internal energy,  $U_{\bar{Q}Q}$ , extracted from the lattice results of the in-medium singlet free energy,  $F_{\bar{Q}Q}^{(1)}$ , in combination with Casimir scaling for the strengths in the non-singlet color channels. Since the long-distance limit of the internal energy,  $U_{\bar{Q}Q}^\infty \equiv U_{\bar{Q}Q}(r \rightarrow \infty)$ , does not go to zero, it needs to be subtracted to ensure the convergence of the scattering equation,

$$V_{\bar{Q}Q}(r) = U_{\bar{Q}Q}(r) - U_{\bar{Q}Q}^\infty. \quad (18)$$

Clearly, for infinite separation in a deconfined medium, the force between 2 quarks should vanish, which is consistent with the leveling off of the free (and internal) energy at large  $r$  in Fig. 7<sup>5</sup>. This energy contribution is naturally associated with an in-medium mass correction (in fact, in the vacuum, it can be identified with the difference between the bare charm-quark and the  $D$ -meson mass). However, an open problem is the entropy contribution in the internal energy,  $U_{\bar{Q}Q} = F_{\bar{Q}Q} + TS_{\bar{Q}Q}$ , which does not vanish for  $r \rightarrow \infty$ ; especially

<sup>5</sup>Recall that the force is the gradient of the potential,  $\vec{F} = -\vec{\nabla}V(r)$

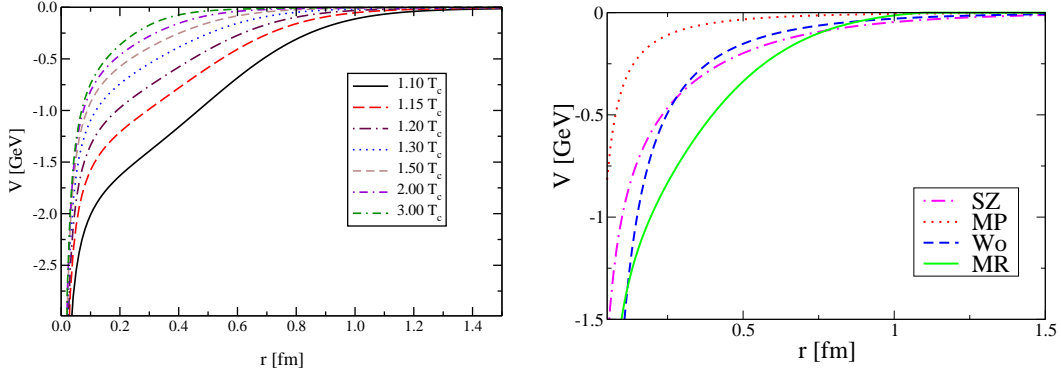


Figure 17: Left panel: subtracted color-singlet heavy-quark internal energy,  $U_{Q\bar{Q}}(r) - U_{Q\bar{Q}}^\infty$ , numerically evaluated from  $N_f=2$  lattice QCD computations in Ref. [25], as a function of  $Q-\bar{Q}$  distance for various temperatures (figure taken from Ref. [23]). Right panel: Comparison [20] of different extractions of the color-singlet  $Q-\bar{Q}$  potential, Eq. (18), at  $T=1.5 T_c$  (SZ= [19], MP= [21], Wo= [24], MR= [20]).

close to the critical temperature, the  $T S_{Q\bar{Q}}^\infty$  term becomes uncomfortably large, and its subtraction consequently leads to a rather strong effective potential, cf. Eq. (18). This is currently the largest uncertainty in the extraction of potentials from the IQCD free energy, which may be as large as 50%, as illustrated in Fig. 17. The use of the internal energy may be regarded as an upper estimate for the strength of the thus constructed potentials.

The numerical calculations of the in-medium heavy-light  $T$ -matrices in the scheme outlined above [60] have found that the dominant interactions are operative in the attractive color-singlet (mesons) and color-antitriplet (diquark) channels, while they are strongly suppressed in the repulsive sextet and octet channels. This can be understood from the iterative structure of the  $T$ -matrix Eq. (13), implying that higher order terms in the Born series,  $T = V + VGV + VGVGV + \dots$ , are of alternating sign for repulsive potentials, while they add for attractive potentials. Moreover, from the left panel of Fig. 18 one sees that the color-singlet meson channel supports charm-light quark resonance structures in the vicinity of the 2-body threshold up to temperatures of possibly  $\sim 1.5 T_c$ , and up to  $\sim 1.2 T_c$  in the antitriplet diquark channel (all numerical results related to the  $T$ -matrix approach as shown here and below are based on the potential labelled “Wo” in the right panel of Fig 17).

The interaction strength may be better quantified via the HQ self-energies, displayed in the right panel of Fig. 18 for charm quarks. While the real parts are small at all temperatures (not exceeding 0.02 GeV), the imaginary parts are substantial, translating into scattering rates (or quasiparticle widths) of up to  $\Gamma_c = -2 \text{Im}\Sigma_c \simeq 0.2\text{-}0.3$  GeV not too far above  $T_c$ . Part of the reason for the different magnitudes in real and imaginary parts is that the real part of the  $T$ -matrix assumes both positive (repulsive) and negative (attractive) values, which compensate each other when integrated over (or from different channels). The imaginary part of the  $T$ -matrix is strictly negative (absorptive) and always adds in the self-energy.

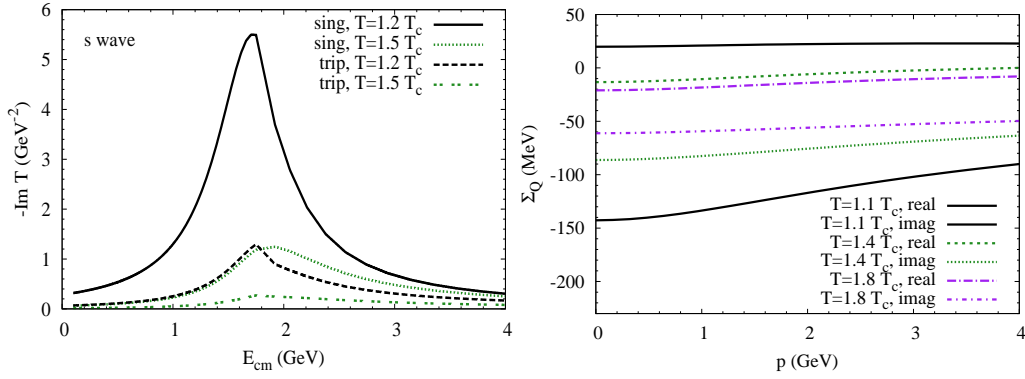


Figure 18: Left panel: in-medium  $T$ -matrix for HQ potential scattering off light quarks and antiquarks in the QGP in the color-antitriplet diquark and color-singlet meson channels, respectively, at 2 different temperatures [60]; right panel: real and imaginary parts of charm-quark self-energies at different temperatures resulting from a sum over all  $T$ -matrix channels; the real parts are generally small, while the imaginary parts are related to the scattering rate by  $\Gamma_c = -2 \text{Im}\Sigma_c$ .

In the following Section we will set up a Brownian-Motion framework for HQ diffusion in the QGP and address the question of how the different interactions we have discussed above reflect themselves in the thermal relaxation for charm and bottom quarks.

### 3.2 Heavy-Quark Transport

The description of the motion of a heavy particle in a fluid (or heat bath) has a long history and a wide range of applications, including problems as mundane as the diffusion of a drop of ink in a glass of water. A suitable approach is given in terms of a diffusion equation for the probability density,  $\rho_1$ , of the “test particle” 1. More rigorously, one starts from the full Boltzmann equation for the phase space density,  $f_1(\vec{r}, \vec{p}, t)$ ,

$$\left( \frac{\partial}{\partial t} + \frac{\vec{p}}{E} \cdot \vec{\nabla}_r - (\vec{\nabla}_r V) \cdot \vec{\nabla}_p \right) f_1(\vec{r}, \vec{p}, t) = I_{\text{coll}}(f_1), \quad (19)$$

where  $\vec{F} = -\vec{\nabla}_r V$  represents the force on the test particle due to an external (in-medium) potential,  $V$ , and  $I_{\text{coll}}(f_1)$  is the collision integral induced by scattering off particles in the heat bath. The application to heavy-quark motion has first been advocated in Ref. [67]. Neglecting the mean-field term in Eq. (19), and assuming a uniform medium, one can integrate the Boltzmann equation over the spatial coordinates to obtain an equation for the distribution function,  $f_Q$ , of the heavy quark in momentum space,

$$f_Q(\vec{p}; t) \equiv \int d^3r f_Q(\vec{r}, \vec{p}, t), \quad (20)$$

which is solely determined by the collision term,

$$\frac{\partial f_Q(\vec{p}; t)}{\partial t} = I_{\text{coll}}(f_Q), \quad (21)$$

The latter can be written as an integral over all momentum transfers,  $k$ ,

$$I_{\text{coll}}(f_Q) = \int d^3k [w(p+k, k)f_Q(p+k) - w(p, k)f_Q(p)], \quad (22)$$

where the key ingredient is a transition rate,  $w(p, k)$ , for the HQ momentum to change from  $p$  to  $p - k$ . The two terms in the integral represent the scattering of the heavy quark into (“gain term”) and out (“loss term”) of the momentum state  $p$ . The transport equation (21) still constitutes a differential-integral equation for  $f_Q$  which in general is not easily solved. At this point, one can take advantage of the HQ quark mass providing a large scale, so that the momentum  $p$  of the heavy quark can be considered to be much larger than the typical momentum transfer,  $k \sim T$ , imparted on it from the surrounding medium. Under these conditions, the transition rate in Eq. (22) can be expanded for small  $k$ . Keeping the first two terms of this expansion, Eq. (21) is approximated by the Fokker-Planck equation,

$$\frac{\partial f_Q(p, t)}{\partial t} = \frac{\partial}{\partial p_i} \left[ A_i(p) + \frac{\partial}{\partial p_j} B_{ij}(p) \right] f_Q(p, t). \quad (23)$$

where the transport coefficients,  $A_i$  and  $B_{ij}$ , are given by

$$A_i(p) = \int d^3k w(p, k) k_i, \quad B_{ij}(p) = \frac{1}{2} \int d^3k w(p, k) k_i k_j \quad (24)$$

in terms of the transition rate  $w$ ;  $A_i$  encodes the average momentum change of the heavy quark per unit time and thus describes the friction in the medium, while  $B_{ij}$  represents the average momentum broadening per unit time, i.e., the diffusion in momentum-space. For an isotropic medium (in particular a medium in thermal equilibrium), the transport coefficients can be reduced to

$$A_i(p) = \gamma(p^2)p_i, \quad B_{ij}(p) = \left[ \delta_{ij} - \frac{p_i p_j}{p^2} \right] B_0(p^2) + \frac{p_i p_j}{p^2} B_1(p^2), \quad (25)$$

where the friction coefficient  $\gamma = \tau_{\text{therm}}^{-1}$  is equivalent to a thermal relaxation time, and  $B_0$  and  $B_1$  are diffusion coefficients. It is very instructive to examine the limit of momentum independent coefficients (which in general is not the case and will not be assumed below), in which case the Fokker-Planck equation reduces to a particularly simple form,

$$\frac{\partial f_Q}{\partial t} = \gamma \frac{\partial}{\partial p_i} (p_i f_Q) + D \frac{\partial}{\partial p_i} \frac{\partial}{\partial p_i} f_Q, \quad (26)$$

which clearly illustrates the form of the diffusion term, proportional to a single diffusion constant  $D$ . The diffusion and friction constants are, in fact, related via Einstein’s famous fluctuation-dissipation relation,

$$\gamma = \frac{D}{Tm_Q}, \quad (27)$$

reducing the problem to a single transport coefficient. Note the intimate connection between the HQ transport coefficients and the temperature of the surrounding medium. This demonstrates that the Fokker-Planck equation is a consistent approximation to the Boltzmann equation in the sense that it recovers the proper equilibrium limit: both friction and diffusion terms are essential to implement the principle of detailed balance; a “pure” diffusion equation (i.e.,  $\gamma=0$ ) is only applicable in the limit  $T, m_Q \rightarrow \infty$ . Even in the presence of momentum dependent transport coefficients, the Einstein relation (27), remains valid in the zero-momentum limit ( $p \rightarrow 0$ ) and provides for a valuable check whether the computed HQ diffusion constants  $D$  and  $\gamma$  recover the temperature of the ambient medium.

In phenomenological applications to heavy-ion collisions, the evolution of high- $p_T$  particles is often approximated within an energy-loss treatment, which amounts to neglecting the diffusion term, i.e.,  $D \rightarrow 0$ . This means that only momentum- (or energy-) degrading processes are taken into account, which is reflected in the Einstein equation as the  $T \rightarrow 0$  limit (with  $D/T$  finite). The lack of momentum diffusion implies that both momentum randomization and energy-gain processes are neglected. Thus, the particles can neither equilibrate nor become part of the collectively expanding medium (which is, of course, crucial for the transfer of transverse and elliptic flow from the medium to the particles propagating through it). Nevertheless, at high momentum this approximation may be in order if the microscopic processes underlying energy loss are rare and at high momentum transfer. In this case the Fokker-Planck equation is not reliably applicable.

Let us now turn to the microscopic input to the calculation of the transport coefficients. Throughout the remainder of this paper, we employ fixed HQ masses at  $m_c = 1.5$  GeV and  $m_b = 4.5$  GeV. Using Fermi’s Golden Rule of quantum mechanics (or quantum field theory), the transition rate  $w$  can be expressed via the quantum mechanical scattering amplitude,  $\mathcal{M}$ , underlying the pertinent scattering process in the medium. For elastic  $Q + i \rightarrow Q + i$  scattering ( $i = q, \bar{q}, g$ ), the rate can be written as

$$w(p, k) = \int \frac{d_i d^3q}{16(2\pi)^9 \omega_p \omega_q \omega_{q+k} \omega_{p-k}} f_i(q) \overline{|\mathcal{M}_{iQ}|^2} (2\pi)^4 \delta(\omega_p + \omega_q - \omega_{p-k} - \omega_{q+k}) . \quad (28)$$

In perturbative QCD, the amplitude is explicitly given by Eq. (9) representing the Feynman diagrams depicted in Fig. 12. Likewise, the  $T$ -matrix discussed in the previous Section can be directly related to the  $\mathcal{M}$  amplitude, see Ref. [60]. In Eq. (28),  $d_i$  denotes the spin-color degeneracy of the parton,  $f_i(q)$  is its phase-space distribution in the medium, while  $p$  and  $q$  ( $p - k$  and  $q + k$ ) are the initial (final) momenta of the heavy quark and the parton, respectively. All in- and outgoing particles are on their mass shell, i.e.,  $\omega_p = \sqrt{m^2 + p^2}$  with their respective masses,  $m = m_{Q,i}$ ; the  $\delta$ -function enforces energy conservation in the process.

In Fig. 19, we compare the temperature dependence of the inverse friction coefficient (thermal relaxation time) for charm quarks at zero momentum for elastic scattering in pQCD (as discussed in Sec. 3.1.1) with the effective resonance model (Sec. 3.1.2). The latter leads to substantially lower thermalization times than pQCD scattering, by around a factor of  $\sim 3$  at temperatures  $T \simeq 1-2 T_c$ . In contrast to pQCD, the values of  $\tau_{c,\text{therm}} \simeq 2-10$  fm/c within



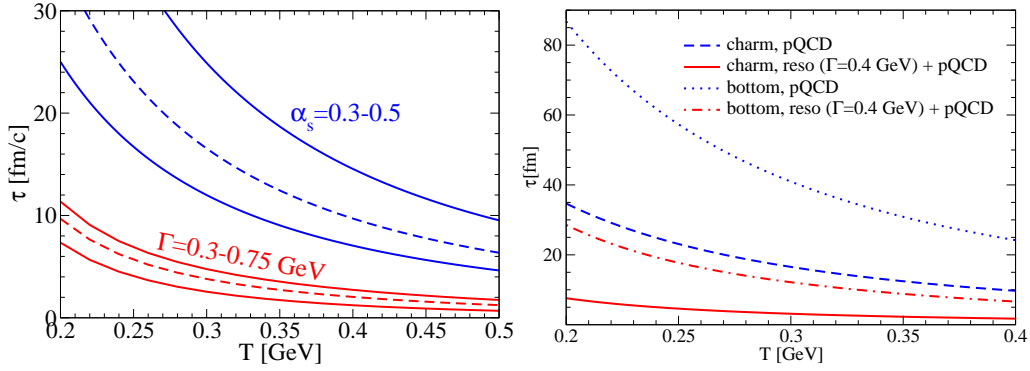


Figure 19: Thermal relaxation times of heavy quarks at zero 3-momentum as a function of temperature in the QGP [42]; left panel: charm quarks in the resonance model (with a  $D$ -meson width  $\Gamma_D=0.3-0.8$  GeV; lower band) compared to LO-pQCD (with a strong coupling constant  $\alpha_s=0.3-0.5$ ; upper band) [75]. Right panel: comparison of resonance+pQCD interactions (red lines) and pQCD only (blue lines) for charm and bottom quarks.

the resonance model are comparable to the expected QGP lifetime at RHIC,  $\tau_{\text{QGP}} \simeq 5 \text{ fm}/c$ ; thus, if resonances are operative, significant modifications of charm spectra at RHIC are anticipated due to (the approach to) thermalization. The uncertainty band covered by varying the effective coupling constant,  $G$ , over a wide range is comparatively moderate. We recall that the magnitude of the underlying total cross sections for pQCD and the resonance model (cf. left panel of Fig. 13) are not largely different; an important effect thus arises due to the angular dependence of the differential cross section (or scattering amplitudes), which is forward dominated in pQCD (corresponding to a small 3- or 4-momentum transfer,  $t$  or  $k$ ) while isotropic in the rest frame of a  $D$ -meson resonance implying larger momentum transfers,  $k$ . Since the expression for  $A_i$  (and thus for  $\gamma$ ), Eqs. (24) and (25), directly involves  $k$ , large-angle scattering is more efficient in thermalizing the  $c$ -quark distributions. Charm-quark relaxation in the resonance model appears to become less efficient at high temperatures. This is not due to the disappearance of the resonances (as will be the case in the lattice-QCD based potential approach), but due to a mismatch between the excitation energy of the resonances and the increasing average thermal energy of the partons in the heat bath. E.g., at  $T = 0.5 \text{ GeV}$ , the latter amounts to  $\omega_{\text{thermal}} = 3 T = 1.5 \text{ GeV}$ , which is well above the optimal energy for forming a  $D$ -meson resonance in collisions with a zero-momentum charm quark. Thus, with increasing temperatures the efficiency of the resonances in  $c$ -quark scattering is diminished since the partons in the surrounding medium become too energetic.

The effect of  $B$ -meson resonances on bottom quarks is relatively similar to the charm sector, i.e., a factor of  $\sim 3$  reduction in the thermal relaxation time compared to pQCD, cf. right panel of Fig. 19. However, the magnitude of  $\tau_{b,\text{therm}}$  stays above typical QGP lifetimes at RHIC, especially below  $2 T_c$  where almost all of the QGP evolution is expected

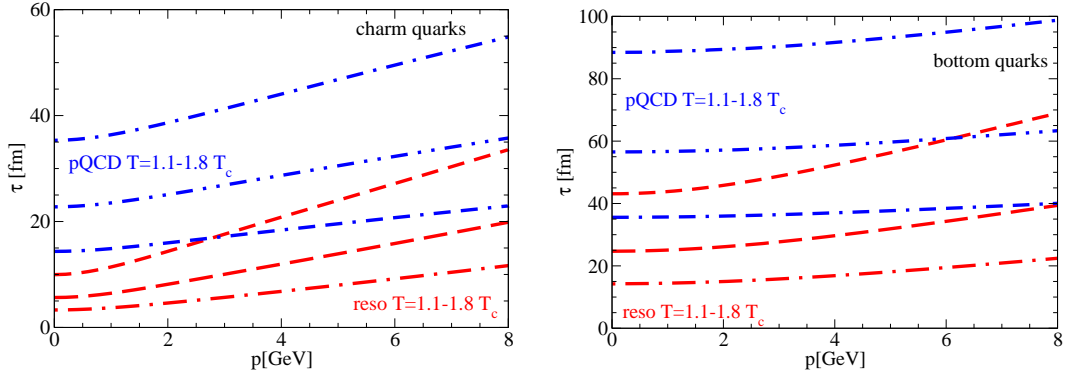


Figure 20: Thermal relaxation times of charm (left panel) and bottom quarks (right panel) in the QGP as a function of 3-momentum at 3 different temperatures, using either pQCD ( $\alpha_s=0.4$ ; upper 3 lines at  $p=0$  for charm, and lines 1, 2 and 4 from above at  $p=0$  for bottom) or resonance scattering ( $\Gamma_\Phi=0.4$  GeV; lower 3 lines at  $p=0$  for charm, and lines 1, 2 and 4 from below at  $p=0$  for bottom) [42]. The temperatures are  $T=1.1 T_c$ ,  $1.4 T_c$  and  $1.8 T_c$  from top to bottom within each set of interaction.

to occur (based, e.g., on hydrodynamic simulations). The momentum dependence of the relaxation times for LO-pQCD and resonance interactions is illustrated in Fig. 20. The latter show a more pronounced increase of the relaxation time with increasing  $p$ , since their interaction strength is concentrated at low energies. It has been found that even at high momenta, the main interaction is still via resonance formation with a “comoving” parton from the heat bath (rather than from tails of the resonance in interactions with partons of typical thermal energies).

Next, we examine the transport coefficients as computed from the  $T$ -matrix approach using IQCD-based potentials (as elaborated in in Sec. 3.1.3). In Fig. 21 we display the temperature dependence of the thermal relaxation time for charm quarks. Close to  $T_c$ , the strength of the  $T$ -matrix based interactions (including all color channels) is very comparable to the effective resonance model. It turns out that the color-singlet meson channel and the color-antitriplet diquark channel contribute to the friction coefficient by about equal parts; the somewhat smaller  $T$ -matrix in the diquark channel is compensated by the 3-fold color degeneracy in the intermediate scattering states. The contribution of the repulsive sextet and octet channels is essentially negligible. Contrary to both pQCD and the resonance model, the IQCD-based  $T$ -matrix approach leads to an increase of the  $c$ -quark relaxation time with increasing temperature, despite the substantial increase of the parton densities with approximately  $T^3$ . The increase in scattering partners is overcompensated by the loss of interaction strength as determined by weakening of the IQCD-based potentials, which is largely attributed to color screening. As a consequence, thermalization due to LO-pQCD scattering becomes more efficient than the nonperturbative  $T$ -matrix for temperatures above  $T \simeq 1.8 T_c$ . This feature is very much in line with the generally expected behavior that

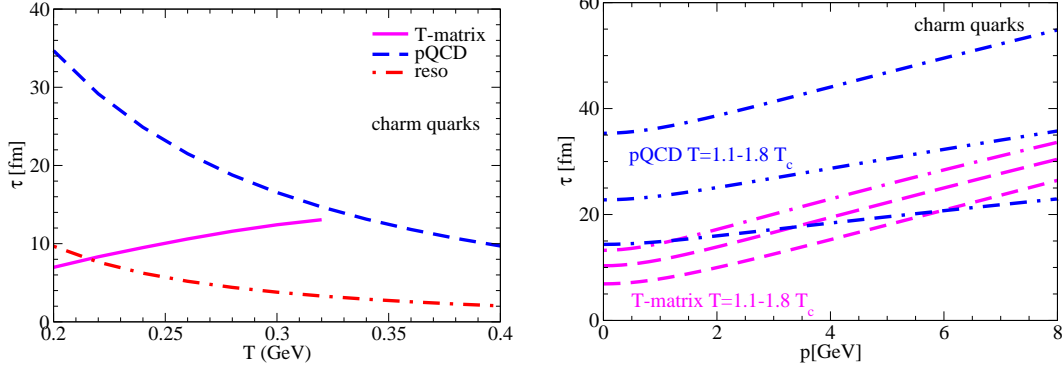


Figure 21: Thermal relaxation times for charm quarks in the QGP as computed from the heavy-light quark  $T$ -matrices utilizing potentials estimated from lattice QCD, including all 4 color combinations in  $c\bar{q}$  and  $cq$  channels [60, 66]. The temperature dependence at zero 3-momentum (middle line in the left panel) and the 3-momentum dependence at 3 temperatures (lower 3 lines at  $p=0$  in the right panel) of  $\tau_{c,\text{therm}}$  are compared to LO-pQCD scattering (upper blue curves at  $p=0$ ). Note that in the right panel, the curves are for temperatures  $T=1.1 T_c$ ,  $1.4 T_c$ ,  $1.8 T_c$  from bottom top (top to bottom) for the  $T$ -matrix (pQCD) interactions.

the QGP becomes a more weakly coupled gas at sufficiently large temperatures. More quantitatively, it is reflected by lattice QCD computations of bulk matter properties, in particular by the so-called “interaction measure”,  $\varepsilon - 3P$ , which may be interpreted as an indicator of nonperturbative effects: as apparent from the left panel of Fig. 5, this quantity becomes close to zero at temperatures above  $\sim 2T_c \simeq 0.4$  GeV. Similarly, up to  $\sim 2T_c$ , the (renormalized) Polyakov loop exhibits substantial deviations from one (i.e., the value corresponding to a “fully” deconfined QGP), cf. right panel of Fig. 6. The 3-momentum dependence of the  $T$ -matrix based relaxation times, shown in the right panel of Fig. 21, reconfirms the loss of interaction strength at high momenta as found in the resonance model. The transport properties of the bottom quarks as evaluated in the  $T$ -matrix approach are summarized in Fig. 22; one finds very similar features as in the charm sector, quantitatively differing by a factor of  $\sim m_b/m_c = 3$ .

The momentum-space diffusion (or friction) coefficient can be converted into a spatial diffusion constant, defined in the standard way via the variance of the time ( $t$ ) evolution of the particle’s position,

$$\langle x^2 \rangle - \langle x \rangle^2 = 2D_x t. \quad (29)$$

with

$$D_x = \frac{dT}{m_Q \gamma} \quad (30)$$

and  $D_s = D_x/d$  where  $d$  denotes the number of spatial dimensions. In Fig. 23,  $D_s$  for charm and bottom quarks is summarized for the 3 different interactions (LO-pQCD, reso-

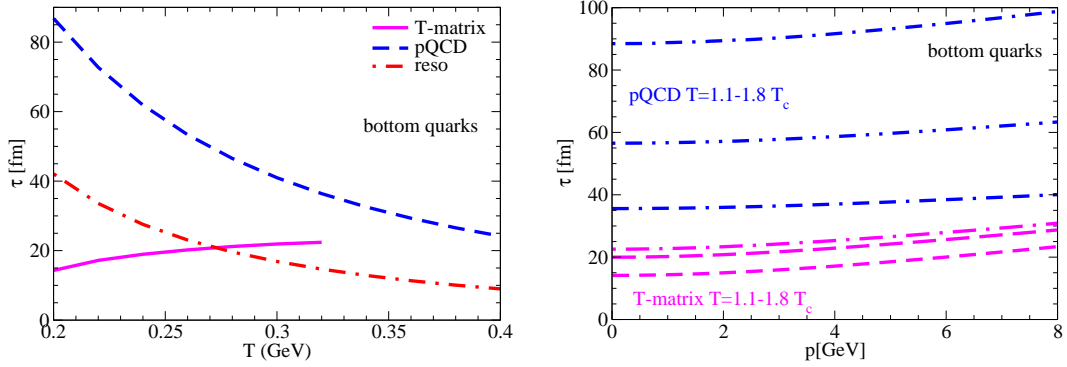


Figure 22: Same as Fig. 21 but for bottom quarks [60, 66].

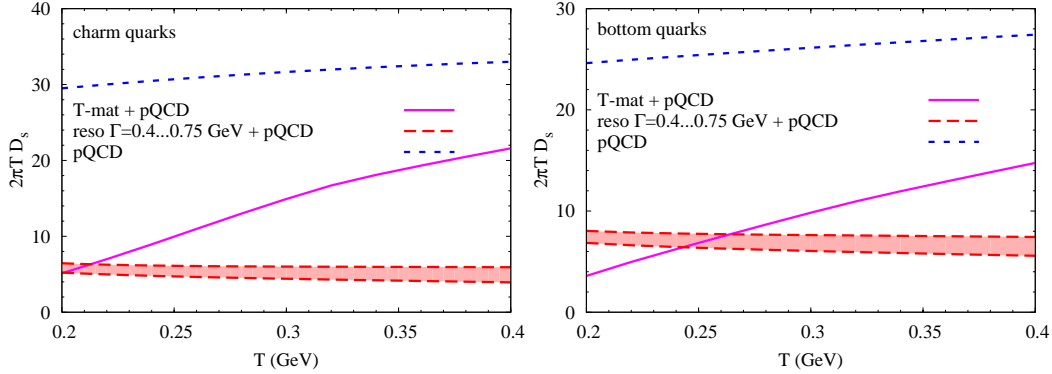


Figure 23: Spatial diffusion constant,  $D_s$ , for charm (left panel) and bottom (right panel) quarks in units of the thermal wave length,  $1/(2\pi T)$ , as a function of temperature. Compared are results from elastic pQCD scattering, resonance+pQCD model and  $T$ -matrix+pQCD model.

nance+pQCD model and nonperturbative  $T$ -matrix+pQCD). Nonperturbative interactions lead to a substantial reduction of diffusion in coordinate space compared to LO pQCD, especially for charm quarks. E.g., for a central Au-Au collision at RHIC, taking as an illustration  $T \simeq 0.2$  GeV,  $t = \tau_{\text{QGP}} \simeq 5$  fm/c,  $D_s = 6/2\pi T$  and  $d = 2$  (in the transverse plane), one finds  $\Delta x = \sqrt{2D_x t} \simeq 4.3$  fm/c compared to  $\sim 8.6$  fm/c for LO pQCD only. This indicates that spatial diffusion is significantly inhibited in the presence of nonperturbative interactions, and is smaller than the typical transverse size of the fireball,  $R \simeq 8$  fm/c, indicating a strong coupling of the charm quark to the medium over the duration of its evolution.

### 3.3 Heavy-Quark Observables at RHIC

In this Section we elaborate on how the above developed Brownian Motion approach can be implemented into a description of HQ observables in ultrarelativistic heavy-ion collisions (URHICs) [43, 45, 69, 70]<sup>6</sup>. This requires the following ingredients: (i) a realistic evolution of the expanding QGP fireball; (ii) Langevin simulations of the heavy quarks in the fireball background with realistic input spectra; (iii) hadronization of the HQ spectra into  $D$ - and  $B$ -meson spectra at the end of the QGP fireball evolution, and (iv) semileptonic decays of the  $D$ - and  $B$ -mesons to compare to experimental single-electron ( $e^\pm$ ) spectra. We will focus on Au-Au ( $\sqrt{s} = 200$  AGeV) collisions at RHIC where first measurements of the nuclear modification factor,  $R_{AA}(p_T)$ , and elliptic flow,  $v_2(p_T)$ , have become available over the last  $\sim 3$ -4 years.

#### 3.3.1 Langevin Simulations

The Fokker-Planck equation for the time evolution of the phase-space distribution of a heavy particle moving through a fluid can be solved stochastically utilizing a Langevin process. The change in position and momentum of the heavy quark over a discrete but small time interval,  $\delta t$ , are evaluated in the rest frame of the medium (QGP) according to

$$\delta \vec{x} = \frac{\vec{p}}{\omega_p} \delta t, \quad \delta \vec{p} = -A(t, \vec{p} + \delta \vec{p}) \vec{p} \delta t + \delta \vec{W}(t, \vec{p} + \delta \vec{p}), \quad (31)$$

where  $\omega_p$  denotes the on-shell HQ energy and  $\vec{p}/\omega_p$  is its relativistic velocity. The drag and diffusion terms of the Fokker-Planck equation determine the change of momentum,  $\delta \vec{p}$ . The momentum diffusion is realized by a random change of momentum  $\delta \vec{W}$  which is assumed to be distributed according to Gaussian noise [68],

$$P(\delta \vec{W}) \propto \exp \left[ -\frac{\hat{B}_{jk} \delta W^j \delta W^k}{4\delta t} \right], \quad \hat{B}_{ij} = (B^{-1})_{ij}, \quad (32)$$

where  $(B^{-1})_{ij}$  denotes the inverse of the matrix  $B_{ij}$ , the momentum-diffusion coefficients of Eq. (25). The Gaussian form of this force is inherently consistent with the underlying Fokker-Planck equation which was derived from the Boltzmann equation in the limit of many small momentum transfers (central limit theorem).

A realistic application to URHICs hinges on a proper description of the evolving medium. As discussed in Sec. 2.3, ideal hydrodynamic simulations, especially for the QGP phase, reproduce the observed collective expansion properties in central and semi-central Au-Au collisions at RHIC very well, and have been employed for HQ Langevin simulations in connection with LO-pQCD transport coefficients in Ref. [43]. Alternatively, the basic features of hydrodynamic evolutions (collective flow and expansion timescales) may be parametrized using expanding fireball models. In Ref. [45], an earlier developed

<sup>6</sup>For implementations into parton transport models, see, e.g., Refs. [71, 72].

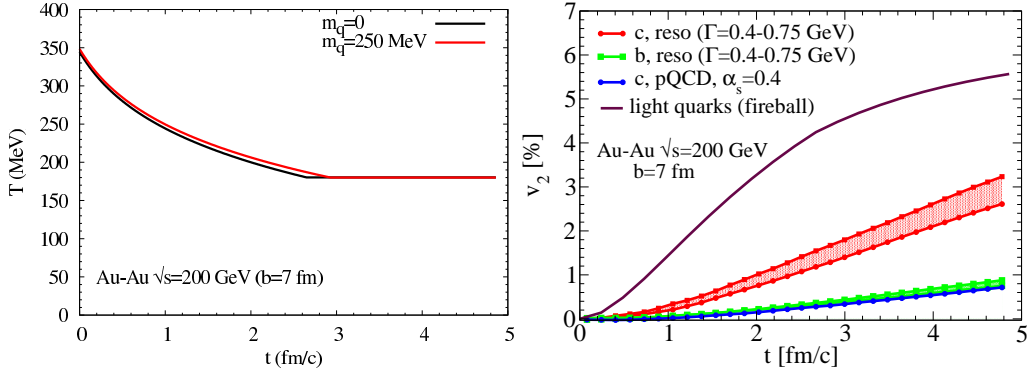


Figure 24: Thermal fireball expansion for semicentral Au-Au collisions at RHIC. Left panel: temperature evolution for either a massless gas with  $d_{\text{eff}}=42$  or a massive quasi-particle gas with  $d_{\text{QGP}}=48$  and thermal parton masses of  $m_i=0.25$  GeV; right panel: time evolution of the inclusive elliptic flow,  $v_2$ , of the bulk medium (upper solid curve) and for heavy quarks as following from relativistic Langevin calculations: charm quarks with LO-pQCD interactions only ( $\alpha_s=0.4$ , lowest line), as well as charm (upper band) and bottom quarks (lower band) for the resonance model ( $\Gamma_D=0.4$  GeV) + pQCD.

fireball model for central Au-Au collisions [73] has been extended to account for the azimuthally asymmetric (elliptic) expansion dynamics closely reminiscent of the hydrodynamic simulations of Ref. [74]. Let us briefly outline the main components of such a description. The starting point is the time dependent volume expansion of a fire cylinder,  $V_{\text{FB}} = z(t)\pi a(t)b(t)$  where  $a(t)$  and  $b(t)$  characterize the elliptical expansion in the transverse plane and  $z(t)$  the longitudinal size (typically covering  $\Delta y = 1.8$  units in rapidity, corresponding to the width of a thermal distribution). As in ideal hydrodynamics, the evolution is assumed to be isentropic, i.e., to proceed at a fixed total entropy,  $S$ , which is matched to the number of observed hadrons at the empirically inferred chemical freezeout, cf. Fig. 2. The time dependence of the entropy density,  $s(t) = S/V_{\text{FB}}(t) = s(T)$ , then determines the temperature evolution,  $T(t)$  of the medium using  $s_{\text{QGP}}(T) = d_{\text{eff}} \frac{4\pi^2}{90} T^3$  in the QGP (with  $d_{\text{eff}} \simeq 40$  to account for deviations from the ideal gas, cf. Fig. 5) and a (numerical) hadron resonance gas equation of state,  $s_{\text{HG}}(T)$ , in the hadronic phase. At  $T_c$ , which at RHIC energies is assumed to coincide with chemical freezeout at  $T_{\text{chem}} = 180$  MeV, the hadron gas is connected to the QGP phase in a standard mixed-phase construction. Assuming a formation time of the thermal medium of  $\tau_0 = 1/3$  fm/c (translating into a longitudinal size of  $z_0 = \tau_0 \Delta y = 0.6$  fm) after the initial overlap of the colliding nuclei, the initial temperature for semicentral (central) Au-Au( $\sqrt{s} = 200$  AGeV) collisions amounts to  $T_0 = 0.34(0.37)$  GeV. The subsequent cooling curve and elliptic flow of the bulk medium are displayed in Fig. 24. The last ingredient needed for the HQ Langevin simulations are the initial charm and bottom-quark spectra. They have been constructed to reproduce available experimental information on  $D$ -meson and  $e^\pm$  spectra in elementary  $p$ - $p$  and  $d$ -Au colli-

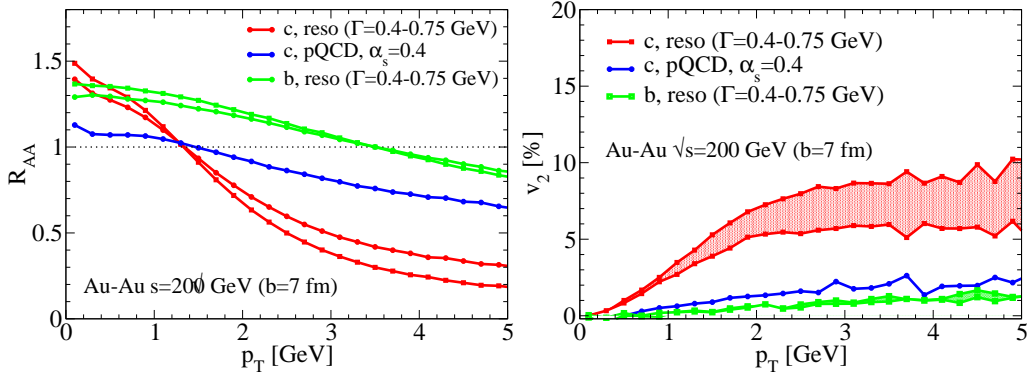


Figure 25: Nuclear modification factor (left panel) and elliptic flow (right panel) of heavy quarks as a function of their transverse momentum in semicentral ( $b=7$  fm) Au-Au collisions [45].

sions at RHIC [75], where no significant medium formation (and thus modification of their production spectra) is expected.

In Fig. 25 we compare the results for HQ  $p_T$  spectra and elliptic flow of Langevin simulations in the above described fireball expansion using either LO-pQCD scattering with  $\alpha_s = 0.4$  (which may be considered as an upper estimate) or a combination of the  $Q + \bar{q} \rightarrow \Phi$  resonance interaction with LO-pQCD [45]. This combination is motivated by the fact that in the resonance model the interaction of a heavy quark is restricted to (light) antiquarks from the medium, while LO-pQCD is dominated by interactions with thermal gluons (the contribution from antiquarks is small, at the  $\sim 10$ -15% level of the total pQCD part). One finds that both the suppression at intermediate  $p_T$  and the elliptic flow of charm quarks are augmented by a factor 3-5 over LO-pQCD interactions, quite reminiscent to what has been found at the level of the transport coefficients. The uncertainty due to variations in the effective resonance parameters is moderate, around  $\pm 30\%$ . It is remarkable that the Langevin simulations naturally provide for a leveling off of the elliptic flow as a characteristic signature of the transition for a quasi-thermal regime at low  $p_T$  to a kinetic regime for  $p_T \geq 2$  GeV, very reminiscent to the empirical  $KE_T$  scaling shown in Fig. 10. Even the quantitative plateau value of 7-8% is recovered, indicating that with the resonance+pQCD model the  $c$ -quarks are largely participating in the collective expansion of the medium. On the other hand, bottom quarks strongly deviate from the universal behavior, which is of course due to their much larger mass,  $m_b = 4.5$  GeV.

The results of the HQ Langevin calculations in a hydrodynamic simulation for semicentral Au-Au collisions are summarized in Fig. 26 [43]. In these calculations, the pQCD HQ scattering amplitudes have been augmented by a full perturbative in-medium gluon exchange propagator with a fixed Debye mass of  $\mu_D = 1.5 T$ , while the strong coupling constant  $\alpha_s$  has been varied to produce a rather large range of diffusion constants. The hydrodynamic evolution is performed for Au-Au collisions at impact parameter  $b=6.5$  fm

with a thermalization time of  $\tau_0=1$  fm/c (corresponding to an initial temperature of  $T_0 = 0.265$  GeV) and a critical temperature of  $T_c=0.165$  GeV. The basic trends of the HQ spectra and elliptic flow are consistent with the fireball simulations of Ref. [45], indicating a strong correlation between large  $v_2$  and small  $R_{AA}$  (strong suppression). Comparing more quantitatively the simulations with a “realistic” pQCD HQ diffusion constant of  $D_s = 24/2\pi T$  to LO-pQCD in the fireball evolution (corresponding to  $D_s \simeq 30/2\pi T$ ), reasonable agreement is found, with  $R_{AA}(p_T=5 \text{ GeV})\simeq 0.7$  and  $v_2(p_T=5 \text{ GeV})\simeq 1.5\text{-}2 \%$ , especially when accounting for the lower  $T_0$  in the hydro evolution (implying less suppression) and the smaller impact parameter (implying less  $v_2$ ).

It is very instructive to investigate the time evolution of the suppression and elliptic flow, displayed in Fig. 27 for the resonance+pQCD model in the fireball evolution. It turns out that the suppression in  $R_{AA}$  is actually largely built up in the early stages of the medium expansion, where the latter is the hottest and densest, i.e., characterized by a large (local) opacity. On the other hand, the elliptic flow, being a collective phenomenon, requires about  $\sim 4$  fm/c to build up in the ambient fireball matter, implying that the charm-quark  $v_2$  starts building up only 1-1.5 fm/c after thermalization, and then rises rather gradually, see left panel of Fig. 24. Thus, the time evolution of  $R_{AA}$  and  $v_2$  is not much correlated, quite contrary to the tight correlation suggested by the final results. This will have important consequences for the interpretation of the experimental data in Sec. 3.3.2.

Finally, we show in Fig. 28 the fireball simulation results for heavy quarks in the non-perturbative  $T$ -matrix approach augmented by LO-pQCD scattering. Here, the latter only includes gluonic interactions to strictly avoid any double counting with the perturbative (Born) term of the  $T$ -matrix (which involves scattering off both quarks and antiquarks from the heat bath). The results are very similar to the effective resonance+pQCD model.

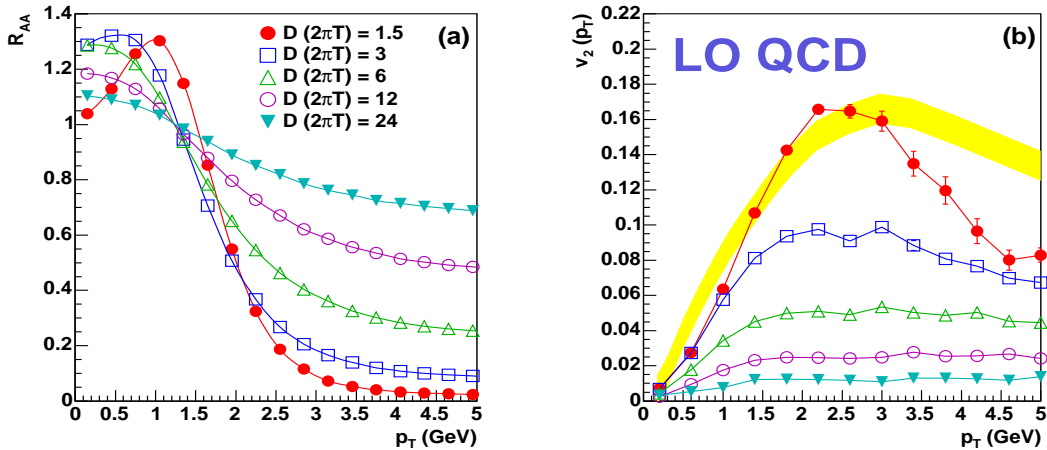


Figure 26: Nuclear modification factor and elliptic flow of charm quarks as a function of their transverse momentum in semicentral ( $b=6.5$  fm) Au-Au collisions using a hydrodynamic evolution of the bulk medium at RHIC [43].



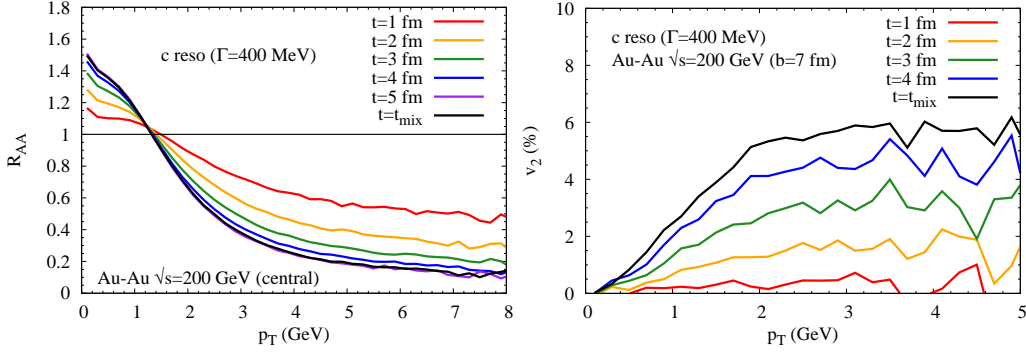


Figure 27: Time evolution of the nuclear modification factor (left panel, central collisions) and elliptic flow (right panel, semicentral collisions) of charm quarks in the resonance+pQCD model in Au-Au collisions at RHIC [45, 56].

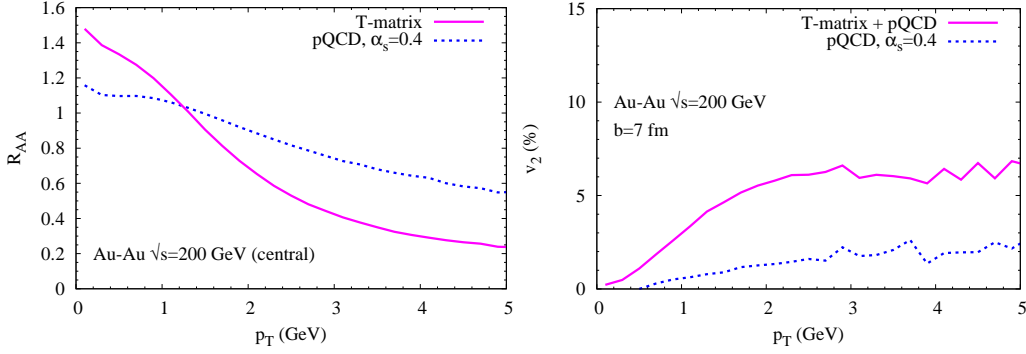


Figure 28: Nuclear modification factor (left panel) and elliptic flow (right panel) of charm quarks in central/semicentral Au-Au collisions at RHIC as computed within HQ Langevin simulations in a thermal fireball background with nonperturbative potential scattering off thermal quarks and antiquarks plus LO-pQCD scattering off gluons [60, 66].

### 3.3.2 Heavy-Meson and Single-Electron Spectra

To make contact with experiment, the quark spectra as computed in the previous section require further processing. First, the quarks need to be converted into hadrons ( $D$  and  $B$  mesons, their excited states, and possibly baryons containing heavy quarks). Second, since the current RHIC data are primarily for single electrons, the pertinent semileptonic decays,  $D, B \rightarrow e\nu_e X$ , need to be evaluated.

The hadronization of quarks produced in energetic collisions of elementary particles (e.g.,  $e^+e^-$  annihilation or hadronic collisions) is a notoriously difficult problem that has so far evaded a strict treatment within QCD and thus requires phenomenological input. A commonly employed empirical procedure to describe hadronization of quarks produced at large

transverse momentum is to define a fragmentation function,  $D_{h/i}(z)$ , which represents a probability distribution that a parton,  $i$ , of momentum  $p_i$  hadronizes into a hadron,  $h$ , carrying a momentum fraction  $z = p_h/p_i$  of the parent parton (with  $0 < z \leq 1$ , reflecting the fact that color-neutralization in the fragmentation process requires the production of extra “soft” partons, which, in general, do not end up in  $h$ ). At large enough  $p_T$ , the parton production occurs at a very short time scale,  $\tau_{\text{prod}} \simeq 1/p_T$ , and thus hadronization, characterized by a typical hadronic scale,  $\tau_{\text{had}} \simeq 1/\Lambda_{\text{QCD}}$ , becomes independent of the production process (this is roughly the essence of the “factorization theorem” of QCD [76]). Therefore, the distribution  $D(z)$  is supposed to be universal, i.e., can be determined (or fit) in, e.g.,  $e^+e^- \rightarrow \text{hadrons}$  and then be applied to hadronic collisions. For light quarks and gluons,  $D(z)$  is typically a rather broad distribution centered around  $z \simeq 0.5$ , while for heavy quarks it is increasingly peaked toward  $z = 1$ , sometimes even approximated by a Dirac  $\delta$ -function,  $D(z) = \delta(z - 1)$  (so called  $\delta$ -function fragmentation). Toward lower  $p_T$ , other hadronization processes are expected to come into play. In hadronic collisions, a possibility is that a produced quark recombines with another quark or antiquark from its environment, e.g., valence quarks of the colliding hadrons [77]. There is ample empirical evidence for the presence (and even dominance) of the recombination mechanism in both  $p$ - $p$  and  $\pi$ - $p$  collisions, in terms of flavor asymmetries of hadrons (including charmed hadrons [78–80]) produced at forward/backward rapidities, where recombination with valence quarks is favored). E.g., for charm production in  $\pi^-N$  collisions, the  $D^-/D^+$  ratio is enhanced at large rapidity,  $y$ , indicating the presence of  $\bar{c}d \rightarrow D^-$  recombination with a  $d$ -quark from the  $\pi^- = d\bar{u}$  (but not  $c\bar{d} \rightarrow D^+$ ).

As discussed in Sec. 2.3, the quark recombination (or coalescence) model has received renewed interest in the context of RHIC data, by providing a successful explanation of 2 phenomena observed in intermediate- $p_T$  hadron spectra, namely the constituent quark-number scaling of the elliptic flow and the large baryon-to-meson ratios. It is therefore natural to also apply it to the hadronization of heavy quarks [54, 81], where it appears to be even more suited since the HQ mass provides a large scale relative to which corrections to the coalescence model are relatively suppressed even at low momentum. We here follow the approach of Ref. [54] where the  $p_T$  spectrum of a  $D$ -meson is given in terms of the light and charm quark or antiquark phase space distributions,  $f_{\bar{q},c}$ , as

$$\frac{dN_D^{\text{coal}}}{dy d^2p_T} = g_D \int \frac{p \cdot d\sigma}{(2\pi)^3} \int d^3q f_D(q, x) f_{\bar{q}}(\vec{p}_{\bar{q}}, \vec{r}_{\bar{q}}) f_c(\vec{p}_c, \vec{r}_c), \quad (33)$$

where  $\vec{p} = \vec{p}_{\bar{q}} + \vec{p}_c$  denotes the momentum of the  $D$  meson,  $g_D$  a combinatorial factor (ensuring color-neutrality and spin-isospin averaging),  $f_D(q, x)$  the Wigner function of the  $D$ -meson which is usually assumed to be a double Gaussian in relative momentum,  $\vec{q} = \vec{p}_c - \vec{p}_{\bar{q}}$  and size,  $\vec{r} = \vec{r}_c - \vec{r}_{\bar{q}}$ , and  $d\sigma$  represents an integration over the hadronization volume. The charm-quark distribution function is directly taken from the output of the Langevin simulations discussed in the previous section, while the light-quark distributions are taken as determined from the successful application of the coalescence model of Ref. [46] to light hadron observables at RHIC. The coalescence mechanism, however, does

not exhaust all charm quarks for hadronization, especially at high  $p_T$  where the light-quark phase-space density becomes very small; in Ref. [45], the “left-over” charm quarks,  $\hat{N}_c$ , have been hadronized with  $\delta$ -function fragmentation (as was done when constructing the input spectrum in connection with  $p$ - $p$  and  $d$ -Au data). The total  $D$ -meson spectrum thus takes the form

$$\frac{dN_D^{\text{tot}}}{dy d^2p_T} = \frac{dN_D^{\text{coal}}}{dy d^2p_T} + \frac{d\hat{N}_c^{\text{frac}}}{dy d^2p_T}. \quad (34)$$

In the approach of Ref. [45] the formation of baryons containing charm quarks (most notably  $\Lambda_c = udc$ ) has been estimated to be rather small, with a  $\Lambda_c/D$  ratio significantly smaller than 1, and is therefore neglected. The same procedure as for charm quarks is also applied for bottom-quark hadronization. In principle, the QGP and mixed phase is followed by an interacting hadronic phase (cf. Fig. 9), where  $D$  and  $B$  mesons are subject to further reinteractions. In Ref. [82]  $D$ -meson reaction rates,  $\Gamma_D^{\text{HG}}$ , have been estimated in a hot pion gas. Even at temperatures close to  $T_c \simeq 0.18$  GeV,  $\Gamma_D^{\text{HG}} \leq 0.05$  GeV, which is significantly smaller than in the QGP at all considered temperatures, cf. Fig. 18, and are therefore neglected in the calculations of Ref. [45]. Finally, the  $D$ - and  $B$ -meson spectra are decayed with their (weighted average) semileptonic decay branching ( $\sim 10\%$  for  $D$  mesons), assuming a dominance of 3-body decays (e.g.,  $D \rightarrow K e \nu$ ). Before discussing the pertinent single- $e^\pm$  spectra in more detail, two important features should be recalled: (i) the shape and magnitude of the decay electrons closely follows those from the parent  $D$  mesons [54, 55]; (ii) the electron spectra are a combination of charm and bottom decays which experimentally have not yet been separated. Since bottom-quark spectra (and thus their decay electrons) are predicted to be much less modified than charm spectra, a reliable interpretation of the  $e^\pm$  spectra mandates a realistic partitioning of the 2 contributions. Following the strategy of Ref. [45], the input charm and electron spectra are constructed as follows: one first reproduces available  $D$ -meson spectra in  $d$ -Au collisions [83], calculates the pertinent electron decays and then adjusts the bottom contribution to reproduce the  $e^\pm$  spectra in  $p$ - $p$  and  $d$ -Au reactions. As a result of this procedure, the bottom contribution to the  $e^\pm$  spectra in the elementary system exceeds the charm contribution at momenta  $p_T \simeq 5$ - $5.5$  GeV, see left panel of Fig. 29; this is consistent with the (rather large) margin predicted by perturbative QCD [86].

The first comparison of the  $e^\pm$  spectra obtained within the Langevin resonance+pQCD+coalescence model [45, 75] to RHIC data available at the time is shown in the middle and right panel of Fig. 29. While no quantitative conclusions could be drawn, a calculation with pQCD elastic scattering alone was disfavored. One also notices that the bottom contribution leads to a significant reduction of the  $v_2^e$  at  $p_T \geq 3$  GeV, as well as a reduced suppression in  $R_{AA}^e$ , where the  $c$  and  $b$  contributions become comparable for  $p_T \geq 4.5$  GeV in semicentral collisions.

The resonance+pQCD+coalescence model is compared to improved  $e^\pm$  data [90–92] in the upper panels of Fig. 30. For central Au-Au collisions, the  $e^\pm$  suppression appears to be underpredicted starting at  $p_T \simeq 4$ - $5$  GeV (with the  $b$  contribution exceeding the charm at  $p_T \geq 3.7$  GeV), indicating the presence of additional suppression mecha-

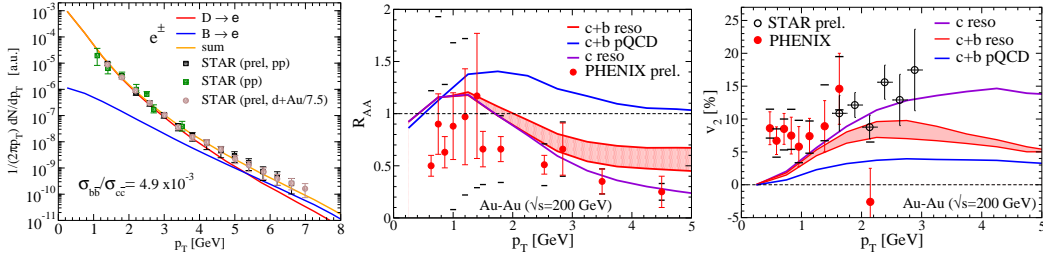


Figure 29: Left panel: single-electron spectra from heavy-flavor decays in  $p$ - $p$  and  $d$ -Au collisions; the empirically inferred decomposition [45, 75] is compared to STAR data [84, 85]. Middle and right panel:  $e^\pm$  elliptic flow and nuclear modification factor in semicentral Au-Au collisions ( $b=7\text{fm}/c$ ) [45, 75] compared to first RHIC data [87–89].

nisms at higher momenta. The lower panels in Fig. 30 show the results of calculations without quark coalescence, i.e., all  $c$  and  $b$  quarks are hadronized with  $\delta$ -function fragmentation. The shape of the  $R_{AA}^e(p_T)$ , as well as the magnitude of  $v_2^e$ , are not properly reproduced. This conclusion has been consolidated by another improvement of the experimental results, displayed in the left panel of Fig. 31 together with theoretical predictions within the resonance+pQCD+coalescence model [45], the hydrodynamic Langevin simulations with pQCD-inspired transport coefficients [43], as well as the radiative energy-loss approach with a transport coefficient  $\hat{q}=14\text{ GeV}^2/\text{fm}$  [53]. Both Langevin simulations point at a HQ diffusion coefficient of around  $D_s \simeq 5/(2\pi T)$ , cf. Fig. 23. The comparison of the 2 Langevin approaches reiterates the importance of the coalescence contribution: the latter is absent in the hydro calculations of Ref. [43] which cannot simultaneously describe the measured elliptic flow and suppression with a single value of the diffusion coefficient. Quark coalescence, on the other hand, introduces an “anti-correlation” of  $v_2$  and  $R_{AA}$  into the spectra which increases the  $v_2$  but decreases the suppression (larger  $R_{AA}$ ), which clearly improves on a consistent description of the data. In the radiative energy loss approach [53], the suppression is approximately reproduced but the azimuthal asymmetry is too small, especially at low  $p_T$ . As discussed in connection with the Fokker-Planck Eq. (26), energy-loss calculations do not account for momentum diffusion; a non-zero  $v_2$  is therefore solely due to the geometric path length difference across the long and the short axes of the almond-shaped transverse fireball area (a shorter path length inducing less suppression). The lack of  $v_2$  thus corroborates the interpretation that the charm (and maybe bottom) quarks become part of the collectively expanding medium, while the large transport coefficient supports the strongly coupled nature of the medium, even without diffusion and coalescence.

Finally, the right panel of Fig. 31 shows the predictions of fireball Langevin simulations employing the nonperturbative  $T$ -matrix+pQCD+coalescence approach for HQ interactions [60]; the agreement with PHENIX data is fair. One should keep in mind that the inherent uncertainties in this approach, e.g., in the extraction and definition of an in-medium two-body potential from the lattice-QCD free energy, are still appreciable, estimated at around  $\pm 30\%$  at the level of  $e^\pm$  observables [60]. A conceptually attractive feature of

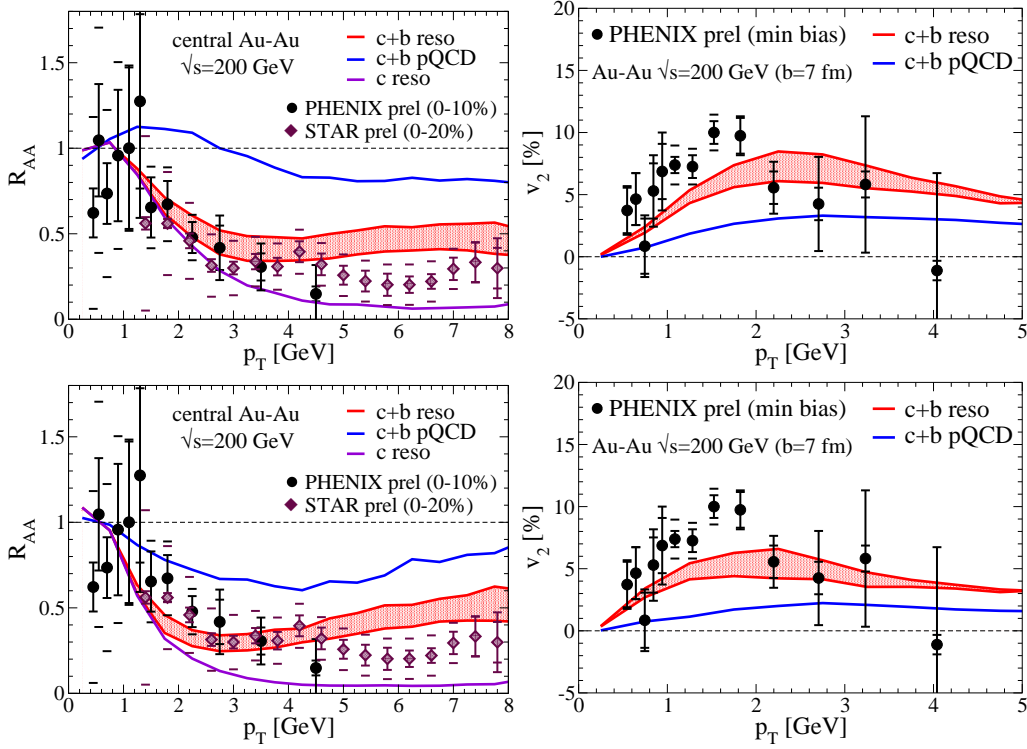


Figure 30: Elliptic flow and nuclear modification factor of electrons from heavy-flavor decays in Au-Au collisions at RHIC as computed within HQ Langevin simulations in a thermal fireball background employing the resonance+pQCD model for HQ interactions in the QGP [45, 56]. In the lower panels, quark coalescence processes at hadronization are switched off. The data are from Refs. [90–92].

the  $T$ -matrix+coalescence approach is that it directly connects two thus far disconnected phenomena observed at RHIC, namely the strongly coupled QGP and quark coalescence: the very same interaction that induces the strong coupling of the heavy quarks to the QGP leads to the formation of “pre-hadronic” resonance structures close to  $T_c$ . The latter are naturally identified with the meson ( $M$ ) and diquark ( $dq$ ) states building up hadrons in a  $q + \bar{q} \rightarrow M$  and  $q + q \rightarrow dq, dq + q \rightarrow B$  processes ( $B$ : baryon), as suggested by the universal constituent-quark number scaling (CQNS), see also Ref. [50].

### 3.4 SQGP at RHIC?

Let us now try to elaborate on the possible broader impact of the current status of the HQ observables and their interpretation. It is gratifying to see that the available electron data thus far confirm the strongly coupled nature of the QGP produced at RHIC; relativistic Langevin simulations have quantified this notion in terms of extracted transport coefficients

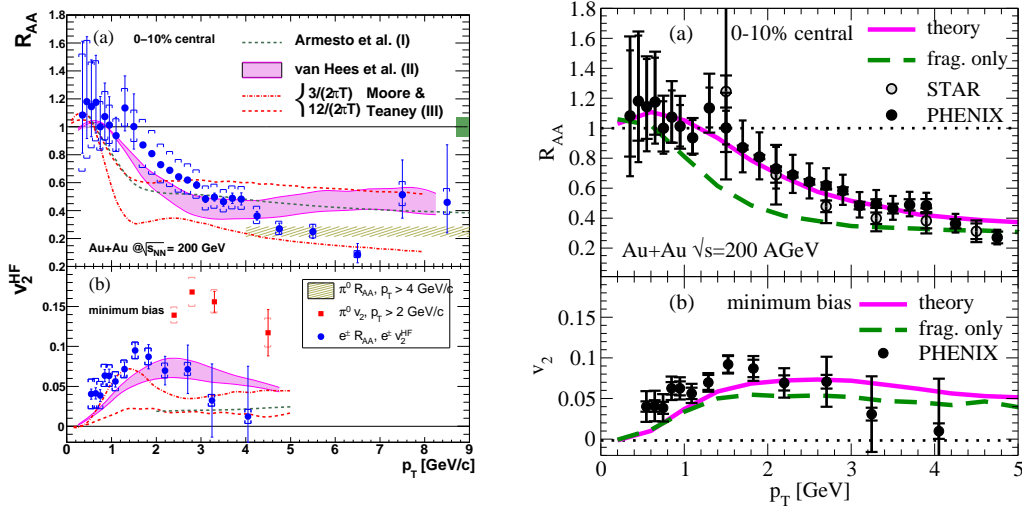


Figure 31: Elliptic flow and nuclear modification factor of electrons from heavy-flavor decays in Au-Au collisions at RHIC. Left panel: PHENIX data [93] compared to theoretical predictions based on the Langevin simulations in the resonance+pQCD+coalescence model (bands) [45] or with upscaled pQCD interactions (dash-dotted and dotted lines) [43], as well as with radiative energy-loss calculations (dashed lines) [53]. Right panel: PHENIX [93] and STAR [94] are compared to Langevin simulations employing HQ  $T$ -matrix interactions plus coalescence [60].

which are a factor of 3-5 stronger than expectations based on elastic perturbative QCD interactions. At least in the low-momentum regime, this should be a reliable statement since the heavy-quark mass warrants the main underlying assumptions, namely: (i) the applicability of the Brownian motion approach, and (ii) the dominance of elastic interactions. Clearly, an important next step is to augment these calculations by a controlled implementation of radiative energy-loss mechanisms, see, e.g., Ref. [95] for a first estimate. As for the microscopic understanding of the relevant interactions underlying the HQ rescattering, it should be noted that large couplings necessarily require resummations of some sort, especially for the problem at hand, i.e., HQ diffusion, for which the perturbation series converges especially poorly [51]. An example of such a (partial) resummation is given by the  $T$ -matrix approach [20, 60] discussed above, which is particularly valuable when it can be combined with model-independent input from lattice QCD. Here the objective must be to reduce the uncertainties in the definition and extraction of a suitable potential. This task can be facilitated by computing “Euclidean” (imaginary time) correlation functions for heavy-light mesons and check them against direct lattice computations which can be carried out with good accuracy. These kinds of constraints are currently pursued in the heavy quarkonium sector [21–23], i.e., for  $Q\bar{Q}$  correlation functions, indicating that potential models are a viable framework to describe in-medium HQ interactions.

An alternative nonperturbative approach to describe the medium of a strongly-coupled

gauge theory has recently been put forward by exploiting connections between string theory and Conformal Field Theory (CFT), the so-called AdS/CFT correspondence. The key point here is a conjectured duality between the weak-coupling limit of a certain string theory (defined in Anti-de-Sitter (AdS) space) and the strong-coupling limit of a supersymmetric gauge theory (“conformal” indicates that the theory does not carry any intrinsic scale, such as  $\Lambda_{QCD}$  in QCD; this difference may, in fact, be the weakest link in the identification of the CFT plasma with the QGP; it implies, e.g., the absence of a critical temperature in CFT). A remarkable result of such a correspondence is the derivation of a universal value for the ratio of shear viscosity to entropy density pertaining to a large class of strongly coupled quantum field theories,  $\eta/s = 1/(4\pi)$ , which was furthermore conjectured to be an absolute lower bound for any quantum liquid [96]. Within the same framework, the HQ diffusion has been computed, with the result  $D_s \simeq 1/(2\pi T)$  [97, 98]. The assumption that the QGP is indeed in a strongly coupled regime (sQGP) can then be utilized to establish a relation between  $\eta/s$  and the heavy-quark diffusion constant, and thus obtain a quantitative estimate of  $\eta/s$ . Based on AdS/CFT, and exploiting the proportionality  $\eta/s \propto D_s$  (as, e.g., borne out of kinetic theory) one has

$$\frac{\eta}{s} \approx \frac{1}{4\pi} D_s (2\pi T) = \frac{1}{2} T D_s \quad (\text{AdS/CFT}) \quad (35)$$

using the empirically inferred  $D_s(2\pi T)=4-6$ , one arrives at  $\eta/s=(4-6)/(4\pi)=(1-1.5)/\pi$ . This may be compared to a rather recent lattice QCD computation displayed in the left panel of Fig. 32 [99], which also contains the result of a perturbative calculation. A caveat here is that the lattice computations are for a pure gluon plasma (GP).

An alternative estimate for  $\eta/s$  might be obtained in the weak-coupling regime. Starting point is a kinetic theory estimate of  $\eta$  for an ultrarelativistic gas [102, 103]

$$\eta \approx \frac{4}{15} n \langle p \rangle \lambda_{\text{tr}}, \quad (36)$$

where  $n$  is the particle density,  $\lambda_{\text{tr}}$  the transport mean free path over which a particle’s momentum is degraded by an average momentum  $\langle p \rangle$ . Assuming the latter to be of order of the average thermal energy of a massless parton, one has  $n \langle p \rangle \approx \varepsilon$  (the energy density of the gas). Further using  $Ts = \varepsilon + P = \frac{4}{3}\varepsilon$  and  $\lambda_{\text{tr}} = \tau_{\text{tr}}$ , one obtains

$$\frac{\eta}{s} \approx \frac{1}{5} T \tau_{\text{tr}}. \quad (37)$$

Finally, accounting for the delayed thermal relaxation time of a heavy quark via  $\tau_Q \approx (T/m_Q)\tau_{\text{tr}}$ , and using the expression, Eq. (30), for the HQ diffusion constant, one arrives at the following rough estimate for a weakly coupled (perturbative) QGP (wQGP),

$$\frac{\eta}{s} \approx \frac{1}{5} T D_s \quad (\text{wQGP}). \quad (38)$$

Note the significantly smaller coefficient in this estimate compared to the one in expression (35), which reflects the expected underestimation of the shear viscosity if a gas estimate

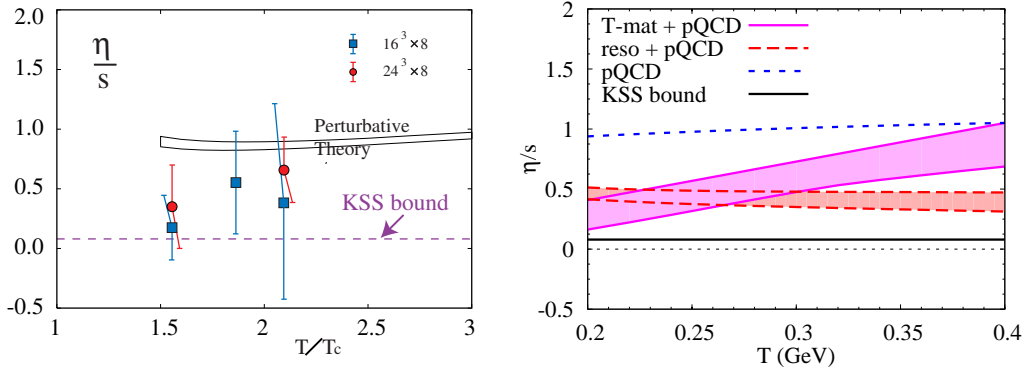


Figure 32: The ratio of shear viscosity to entropy density,  $\eta/s$ . Left panel: lattice QCD computations in a gluon plasma [99] compared to results inferred from perturbation theory [100, 101]. Right panel: schematic estimates utilizing the HQ diffusion constant employing (a) LO pQCD elastic scattering ( $\alpha_s=0.4$ ) in the weakly interacting limit (38) (dashed line), (b) the effective resonance model in the strong-coupling limit (35) (band enclosed by dashed lines), and (c) the lattice-QCD potential based  $T$ -matrix approach (augmented by pQCD scattering off gluons) represented by the band enclosed by solid lines constructed from the weak and strong coupling limits.

is applied in a liquid-like regime (as emphasized in Ref. [102]). As a rough application we may use the LO pQCD results for the HQ diffusion coefficient. With  $D(2\pi T) \simeq 40$  for a gluon plasma (GP) at  $T=0.4$  GeV (see Fig. 23, with a  $\sim 25\%$  increase for removing the contributions from thermal quarks and antiquarks), one finds  $\eta/s \simeq 1.25$ , which is surprisingly close to the perturbative estimate constructed in Ref. [99] which is based on a next-to-leading logarithm of the shear viscosity [101] and a hard-thermal-loop calculation of the entropy density [100] (both of which represent pQCD calculations beyond the LO estimate of the HQ diffusion constant in Fig. 23).

In the right panel of Fig. 32 we attempt a schematic estimate of  $\eta/s$  in the Quark-Gluon Plasma based on the 3 basic calculations of the HQ diffusion coefficient discussed throughout this article. For the LO-pQCD calculation, we adopt the estimate (38) for a weakly coupled gas, while for the resonance+pQCD model we use the strong-coupling estimate (35). The most realistic estimate is presumably represented by the  $T$ -matrix+pQCD calculation, for which we constructed a pertinent band in  $\eta/s$  as follows: the lower limit of the band is based on the weak-coupling estimate, while for the upper limit we adopt the strong-coupling estimate at the low temperature end ( $T=0.2$  GeV), the LO-pQCD only result at the high- $T$  end ( $T=0.4$  GeV) and a linear interpolation in between these 2 temperatures (there are additional uncertainties which are not displayed, e.g., due to the extraction of the lQCD-based interaction potentials).

A remarkable feature of the lattice-QCD potential based  $T$ -matrix approach is that the interaction strength *decreases* with increasing temperature - in other words, the most strongly coupled regime appears to be close to the critical temperature. It turns out that



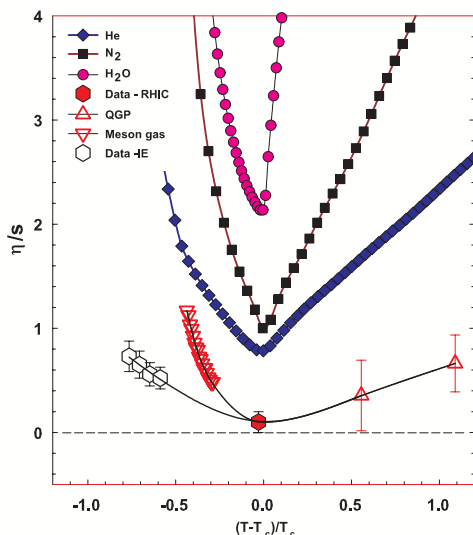


Figure 33: Compilation of the ratio of shear viscosity to entropy density for various substances [104]: atomic He, molecular  $N_2$  and  $H_2O$  [105] (upper 3 symbols), pure-gluon lattice QCD (upward triangles above  $T_c$ ) [99], pion gas (downward triangles below  $T_c$ ) [106] and empirical estimates from heavy-ion data (hexagons) [104].

the occurrence of a maximal interaction strength at a phase transition is a rather generic phenomenon which is present in a large variety of substances: at their critical pressure, helium, nitrogen and even water have a very pronounced minimum in  $\eta/s$  at the critical temperature, as is nicely demonstrated in Ref. [105] and compiled in Fig. 33 taken from Ref. [104]. This plot also contains calculations for  $\eta/s$  in the hadronic phase, using free  $\pi$ - $\pi$  interactions in a pion gas [106] (similar results are obtained for a  $\pi$ - $K$  gas with empirical (vacuum) scattering phase shifts [108]). The decrease of  $\eta/s$  in a hot meson gas with increasing  $T$  corroborates the presence of a minimum around the critical temperature. The finite-temperature QCD phase transition at  $\mu_q=0$  is presumably a cross-over, but the minimum structure of  $\eta/s$  close to  $T_c$  is likely to persist, in analogy to the atomic and molecular system above the critical pressure [105]. If such a minimum is indeed intimately linked to the critical temperature, the AdS/CFT correspondence may be of limited applicability to establish rigorous connections between the sQGP (and RHIC phenomenology) and CFTs, since, as mentioned above, the latter do not possess an intrinsic scale.

The question of how a gluon plasma (GP) compares to a quark-gluon plasma is not merely a theoretical one, but also of practical relevance. In heavy-ion collisions at collider energies (RHIC and LHC), the (very) early phases of the reaction are presumably dominated by the (virtual) gluon fields in the incoming nuclei. A lot of progress has been made in recent years in the determination of these gluon distributions and their early evolution in URHICs [107]. The modifications of the HQ spectra due to these strong “color” fields

should certainly be addressed in future work. In the subsequent evolution, an early formed GP is estimated to chemically equilibrate into a QGP rather rapidly, and closer to  $T_c$  quark coalescence models are suggestive for the dominance of quark degrees of freedom - this is where the  $T$ -matrix approach with IQCD-based potentials is predominantly operative (recall that it hinges on the presence of quarks and antiquarks in the medium). The underlying interactions could therefore provide a unified and quantitative framework for HQ diffusion, quark coalescence and the sQGP in the vicinity of  $T_c$ , based on input which, in principle, is directly extracted from IQCD. Its further development should aim at a better determination of potentials extracted from IQCD, include constraints from lattice correlation functions and applications to quarkonia, and implement contributions due to gluon radiation processes.

## 4 Conclusion and Outlook

The study of elementary particle matter has been an extremely active research field over the last 20-30 years, and it may not have reached its peak time yet. We are beginning to understand better what the key features of media are whose forces are directly governed by gauge theories. Here the strong nuclear force between quarks and gluons (as described by Quantum Chromodynamics) occupies a special role due to its large interaction strength and the self-couplings of its field quanta. On the one hand, QCD gives rise to novel non-perturbative phenomena in the vacuum, most notably the confinement of quarks into hadrons and the chiral symmetry breaking (generating the major part of the visible mass in the universe), whose underlying mechanisms are, however, not yet understood. On the other hand, the Strong Force generates a very rich phase structure of its different matter states (upon varying temperature and baryon density), which are even less understood. Pertinent phase transitions are, in fact, closely connected with deconfinement and chiral symmetry restoration. First principle numerical calculations of discretized (lattice) QCD at finite temperature have clearly established a transition (or a rapid cross over) from hadronic matter into a deconfined Quark-Gluon Plasma with restored chiral symmetry at a temperature of  $T_c \simeq 0.175$  GeV. This state of matter is believed to have prevailed in the early Universe in the first few microseconds after the Big Bang. A particularly exciting aspect of this research field is that such kind of matter can be reproduced, at least for a short moment, in present-day laboratory experiments, by accelerating and colliding heavy atomic nuclei. However, to analyze these reactions, and to extract possible evidence for QGP formation out of the debris of hundreds to thousands of produced hadrons, is a formidable task that requires a broad approach, combining information from lattice QCD, effective models of QCD in a well-defined applicability range, and their implementation into heavy-ion phenomenology. Large progress has been made at the Relativistic Heavy-Ion Collider (RHIC), where clear evidence for the formation of thermalized QCD matter well above the critical energy density has been deduced. The apparently small viscosity of the medium is inconsistent with a weakly interacting gas of quarks and gluons, but is possibly related to recent results from lattice QCD which suggest the presence of resonant correlations for temperatures up to  $\sim 2 T_c$ . We have argued that heavy quarks can serve as controlled probe of the transport

properties of the strongly coupled QGP (sQGP). The modifications of heavy-quark spectra in Au-Au collisions at RHIC can be evaluated in a Brownian motion framework which allows to establish quantitative connections between the heavy-quark diffusion coefficients and observables, such as the suppression of their spectra and especially their elliptic flow. Theoretical analyses have confirmed that perturbative interactions are too weak to account for the measured heavy-quark observables (i.e., their electron decay spectra), while an effective resonance model seems to furnish the required nonperturbative interaction strength. An appealing framework to calculate heavy-quark interactions (and transport properties) in the medium is to extract interaction potentials from lattice QCD and iterate them in a nonperturbative  $T$ -matrix equation. This approach is, in principle, free of adjustable parameters, but currently subject to significant uncertainties, primarily in the definition of the potentials and their applicability to light quarks and at high momentum. However, promising results have been obtained in that the  $T$ -matrix builds up resonance-like structures close to the phase transition, which could be instrumental in explaining the observed elliptic flow. In addition, the resonance correlations naturally explain the importance of quark coalescence processes for the hadronization of the QGP (as indicated by the measured light hadron spectra). Clearly, a lot more work is required to elaborate these connections more rigorously and quantitatively, to implement additional components toward a more complete description (e.g., energy loss via gluon radiation or the effects of strong color fields), to scrutinize the results in comparison to improved lattice QCD computations, and to confront calculations with high precision RHIC (and LHC) data. The latter are expected to emerge in the coming years and will surely hold new surprises, further pushing the frontier of our knowledge of the Quark-Gluon Plasma.

## Acknowledgment

We are indebted to our colleagues Vincenzo Greco, Che-Ming Ko and Massimo Mannarelli for many fruitful discussions and collaboration, and thank William Zajc for a careful reading of the manuscript. This work is supported in part by a U.S. National Science Foundation CAREER award under grant no. PHY-0449489.

## References

- [1] M. Gell-Mann, *Phys. Lett.* **8**, 214 (1964).
- [2] D. J. Gross and F. Wilczek, *Phys. Rev. Lett.* **30**, 1343 (1973).
- [3] H. D. Politzer, *Phys. Rev. Lett.* **30**, 1346 (1973).
- [4] H. Fritzsche, M. Gell-Mann and H. Leutwyler, *Phys. Lett. B* **47**, 365 (1973).
- [5] P. Braun-Munzinger and J. Wambach, arXiv:0801.4256 [hep-ph].

- 
- [6] M. Schmelling, *Proc. of 28. International Conference on High-Energy Physics (ICHEP 96), Warsaw, Poland, 25-31 Jul 1996*, World Scientific, Z. Ajduk and A.K. Wroblewski (eds.), *ICHEP* **96**, 91 (1996); hep-ex/9701002.
- [7] M. Cheng *et al.*, *Phys. Rev. D* **74**, 054507 (2006).
- [8] Y. Aoki, Z. Fodor, S. D. Katz and K. K. Szabo, *Phys. Lett. B* **643**, 46 (2006).
- [9] R. Rapp, T. Schäfer, E. V. Shuryak and M. Velkovsky, *Phys. Rev. Lett.* **81**, 53 (1998).
- [10] M. G. Alford, K. Rajagopal and F. Wilczek, *Phys. Lett. B* **422**, 247 (1998).
- [11] P. Braun-Munzinger, K. Redlich and J. Stachel, in Hwa, R.C. (ed.) et al.: *Quark gluon plasma 3*, 491 (2007); arXiv:nucl-th/0304013.
- [12] M. Cheng *et al.*, arXiv:0710.0354 [hep-lat].
- [13] O. Kaczmarek and F. Zantow, *Phys. Rev. D* **71**, 114510 (2005).
- [14] N. Brambilla *et al.* [Quarkonium Working Group], arXiv:hep-ph/0412158.
- [15] T. Schäfer and E. V. Shuryak, *Rev. Mod. Phys.* **70**, 323 (1998).
- [16] C. E. DeTar and R. Gupta [HotQCD Collaboration], *PoS (LAT2007)* **179** (2007); and arXiv:0710.1655 [hep-lat].
- [17] P. Petreczky and K. Petrov, *Phys. Rev. D* **70**, 054503 (2004).
- [18] S. Digal, P. Petreczky and H. Satz, *Phys. Lett. B* **514**, 57 (2001).
- [19] E. V. Shuryak and I. Zahed, *Phys. Rev. D* **70**, 054507 (2004).
- [20] M. Mannarelli and R. Rapp, *Phys. Rev. C* **72**, 064905 (2005).
- [21] A. Mocsy and P. Petreczky, *Phys. Rev. D* **73**, 074007 (2006).
- [22] W. M. Alberico, A. Beraudo, A. De Pace and A. Molinari, *Phys. Rev. D* **72**, 114011 (2005).
- [23] D. Cabrera and R. Rapp, *Phys. Rev. D* **76**, 114506 (2007).
- [24] C. Y. Wong, *Phys. Rev. C* **72**, (2005) 034906.
- [25] O. Kaczmarek and F. Zantow, arXiv:hep-lat/0506019.
- [26] M. Asakawa, T. Hatsuda and Y. Nakahara, *Prog. Part. Nucl. Phys.* **46**, 459 (2001).
- [27] G. Aarts, C. Allton, M. B. Oktay, M. Peardon and J. I. Skullerud, *Phys. Rev. D* **76**, 094513 (2007);  
M. B. Oktay, M. J. Peardon, J. I. Skullerud, G. Aarts and C. R. Allton, *PoS LAT2007*, 227 (2007).

- 
- [28] M. Asakawa, T. Hatsuda and Y. Nakahara, *Nucl. Phys. A* **715**, 863 (2003).
- [29] F. Karsch and E. Laermann, in Hwa, R.C. (ed.) et al.: *Quark gluon plasma 3*, 1 (2007); arXiv:hep-lat/0305025.
- [30] I. Arsene *et al.* [BRAHMS Collaboration], *Nucl. Phys. A* **757**, 1 (2005);  
B.B. Back *et al.* [PHOBOS Collaboration], *Nucl. Phys. A* **757**, 28 (2005);  
J. Adams *et al.* [STAR Collaboration], *Nucl. Phys. A* **757**, 102 (2005);  
K. Adcox *et al.* [PHENIX Collaboration], *Nucl. Phys. A* **757**, 184 (2005).
- [31] U.W. Heinz and M. Jacob, arXiv:nucl-th/0002042.
- [32] P. Huovinen, P. F. Kolb, U. W. Heinz, P. V. Ruuskanen and S. A. Voloshin, *Phys. Lett. B* **503**, 58 (2001).
- [33] S. Wicks, W. Horowitz, M. Djordjevic and M. Gyulassy, *Nucl. Phys. A* **784**, 426 (2007).
- [34] A. Adare *et al.* [PHENIX Collaboration], *Phys. Rev. Lett.* **98**, 162301 (2007).
- [35] D. Teaney, J. Lauret and E. V. Shuryak, *Phys. Rev. Lett.* **86**, 4783 (2001).
- [36] T. Hirano and K. Tsuda, *Phys. Rev. C* **66**, 054905 (2002).
- [37] P. F. Kolb and U. W. Heinz, in Hwa, R.C. (ed.) et al.: *Quark gluon plasma 3*, 634 (2007); arXiv:nucl-th/0305084.
- [38] C. Nonaka and S. A. Bass, *Phys. Rev. C* **75**, 014902 (2007).
- [39] M. Gyulassy, I. Vitev, X. N. Wang and B. W. Zhang, in Hwa, R.C. (ed.) et al.: *Quark gluon plasma 3*, 69 (2007); arXiv:nucl-th/0302077.
- [40] N. Armesto, C. A. Salgado and U. A. Wiedemann, *Phys. Rev. D* **69**, 114003 (2004).
- [41] R. Baier, *Nucl. Phys. A* **715**, 209 (2003).
- [42] H. van Hees and R. Rapp, *Phys. Rev. C* **71**, 034907 (2005).
- [43] G. D. Moore and D. Teaney, *Phys. Rev. C* **71**, 064904 (2005).
- [44] M. G. Mustafa, *Phys. Rev. C* **72**, 014905 (2005).
- [45] H. van Hees, V. Greco and R. Rapp, *Phys. Rev. C* **73**, 034913 (2006).
- [46] V. Greco, C. M. Ko and P. Levai, *Phys. Rev. Lett.* **90**, 202302 (2003).
- [47] R. J. Fries, B. Müller, C. Nonaka and S. A. Bass, *Phys. Rev. Lett.* **90**, 202303 (2003).
- [48] R. C. Hwa and C. B. Yang, *Phys. Rev. C* **67**, 034902 (2003).

- [49] B. I. Abelev *et al.* [STAR Collaboration], *Phys. Rev. C* **75**, 054906 (2007).
- [50] L. Ravagli and R. Rapp, *Phys. Lett. B* **655**, 126 (2007).
- [51] S. Caron-Huot and G. D. Moore, arXiv:0708.4232 [hep-ph].
- [52] M. Djordjevic, M. Gyulassy and S. Wicks, *Phys. Rev. Lett.* **94**, 112301 (2005).
- [53] N. Armesto, M. Cacciari, A. Dainese, C. A. Salgado and U. A. Wiedemann, *Phys. Lett. B* **637**, 362 (2006).
- [54] V. Greco, C. M. Ko and R. Rapp, *Phys. Lett. B* **595**, 202 (2004).
- [55] X. Dong, S. Esumi, P. Sörensen, N. Xu and Z. Xu, *Phys. Lett. B* **597**, 328 (2004).
- [56] R. Rapp and H. van Hees, *J. Phys. G* **32**, S351 (2006).
- [57] K. Abe *et al.* [Belle Collaboration], *Phys. Rev. D* **69**, 112002 (2004).
- [58] D. Blaschke, G. Burau, T. Barnes, Yu. Kalinovsky and E. Swanson, *Heavy Ion Phys.* **18**, 49 (2003).
- [59] D. Blaschke, G. Burau, Yu. L. Kalinovsky and V. L. Yudin, *Prog. Theor. Phys. Suppl.* **149**, 182 (2003).
- [60] H. van Hees, M. Mannarelli, V. Greco and R. Rapp, arXiv:0709.2884 [hep-ph].
- [61] G. E. Brown, C. H. Lee, M. Rho and E. Shuryak, *Nucl. Phys. A* **740**, 171 (2004).
- [62] M. Döring, K. Hübner, O. Kaczmarek, F. Karsch, *Phys. Rev. D* **75**, 054504 (2007).
- [63] R. Blankenbecler, R. Sugar, *Phys. Rev.* **142**, 1051 (1966).
- [64] R.H. Thompson, *Phys. Rev. D* **1**, 110 (1970).
- [65] R. Machleidt, *Adv. Nucl. Phys.* **19**, 189 (1989).
- [66] H. van Hees, M. Mannarelli, V. Greco, R. Rapp, in preparation.
- [67] B. Svetitsky, *Phys. Rev. D* **37**, 2484 (1988).
- [68] J. Dunkel and P. Hänggi, *Phys. Rev. E* **71**, 016124 (2005).
- [69] P. B. Gossiaux, V. Guiho and J. Aichelin, *J. Phys. G* **32**, S359 (2006).
- [70] W. Liu and C. M. Ko, arXiv:nucl-th/0603004.
- [71] D. Molnar, *J. Phys. G* **31**, S421 (2005).
- [72] B. Zhang, L. W. Chen and C. M. Ko, *Phys. Rev. C* **72**, 024906 (2005).

- 
- [73] R. Rapp, *Phys. Rev. C* **63**, 054907 (2001).
- [74] P. F. Kolb, J. Sollfrank and U. W. Heinz, *Phys. Rev. C* **62**, 054909 (2000).
- [75] R. Rapp, V. Greco and H. van Hees, *Nucl. Phys. A* **774**, 685 (2006).
- [76] J.C. Collins, D.E. Soper, G. Sterman, *Nucl. Phys.* **B263** (1986) 37.
- [77] K.P. Das and R.C. Hwa, *Phys. Lett.* **68B**, 459 (1977).
- [78] V.G. Kartvelishvili, A.K. Likhoded and S.R. Slabospitsky, *Sov. J. Nucl. Phys.* **33** (1981) 434.
- [79] E. Braaten, Y. Jia and T. Mehen, *Phys. Rev. Lett.* **89**, 122001 (2002).
- [80] R. Rapp and E. V. Shuryak, *Phys. Rev. D* **67**, 074036 (2003).
- [81] Z. w. Lin and D. Molnar, *Phys. Rev. C* **68**, 044901 (2003).
- [82] C. Fuchs, B. V. Martemyanov, A. Faessler and M. I. Krivoruchenko, *Phys. Rev. C* **73**, 035204 (2006).
- [83] J. Adams *et al.* [STAR Collaboration], *Phys. Rev. Lett.* **94**, 062301 (2005).
- [84] A. Tai *et al.* [STAR Collaboration], *J. Phys. G* **30**, S809 (2004).
- [85] A.A.P. Suaide *et al.* [STAR Collaboration] *J. Phys. G* **30**, S1179 (2004).
- [86] M. Cacciari, P. Nason and R. Vogt, *Phys. Rev. Lett.* **95**, 122001 (2005).
- [87] S.S. Adler *et al.* [PHENIX Collaboration], *Phys. Rev. C* **72**, 024901 (2005).
- [88] F. Laue *et al.* [STAR Collaboration], *J. Phys. G* **31**, S27 (2005).
- [89] B. Jacak [PHENIX Collaboration], *J. Phys. Conf. Ser.* **50**, 22 (2006).
- [90] S. S. Adler *et al.* [PHENIX Collaboration], *Phys. Rev. Lett.* **96**, 032301 (2006)
- [91] S. A. Butsyk, *Nucl. Phys. A* **774**, 669 (2006)
- [92] J. Bielcik [STAR Collaboration], *Nucl. Phys. A* **774**, 697 (2006)
- [93] A. Adare *et al.* [PHENIX Collaboration], *Phys. Rev. Lett.* **98**, 172301 (2007).
- [94] B. I. Abelev *et al.* [STAR Collaboration], *Phys. Rev. Lett.* **98**, 192301 (2007).
- [95] I. Vitev, A. Adil and H. van Hees, *J. Phys. G* **34**, S769 (2007).
- [96] P. Kovtun, D. T. Son and A. O. Starinets, *Phys. Rev. Lett.* **94**, 111601 (2005).
- [97] C. P. Herzog, A. Karch, P. Kovtun, C. Kozcaz and L. G. Yaffe, *JHEP* **0607**, 013 (2006).

- [98] J. Casalderrey-Solana and D. Teaney, *Phys. Rev. D* **74**, 085012 (2006).
- [99] A. Nakamura and S. Sakai, *Phys. Rev. Lett.* **94**, 072305 (2005).
- [100] J. P. Blaizot, E. Iancu and A. Rebhan, *Phys. Rev. Lett.* **83**, 2906 (1999).
- [101] P. Arnold, G. D. Moore and L. G. Yaffe, *JHEP* **0305**, 051 (2003).
- [102] P. Danielewicz and M. Gyulassy, *Phys. Rev. D* **31**, 53 (1985).
- [103] W. Israel and J.N. Vandalas, *Lett. Nuovo Cim.* **19**, 887 (1970).
- [104] R. A. Lacey and A. Taranenko, *PoS C FRNC2006*, 021 (2006).
- [105] L. P. Csernai, J. I. Kapusta and L. D. McLerran, *Phys. Rev. Lett.* **97**, 152303 (2006).
- [106] J. W. Chen and E. Nakano, *Phys. Lett. B* **647**, 371 (2007).
- [107] L. McLerran, *Nucl. Phys. A* **752**, 355 (2005).
- [108] M. Prakash, M. Prakash, R. Venugopalan and G. Welke, *Phys. Rept.* **227**, 321 (1993).